Multimedia Tools and Applications
https://doi.org/10.1007/s11042-021-11044-2

Survey of denoising, segmentation and classification of magnetic resonance imaging for prostate cancer

Mamta Juneja, et al. *[full author details at the end of the article]*

Received: 28 November 2019 / Revised: 1 March 2021 / Accepted: 5 May 2021
Published online: 22 June 2021

Abstract
Prostate cancer (PCa) has become the second most dreadful cancer in men after lung cancer. Traditional approaches used for treatment of PCa were manual, time consuming and prone to subjective errors. Thus, there is a need for a Computer aided diagnosis system (CADs) consisting of denoising, segmentation, and classification approaches for diagnosis of PCa. CADs may act as a second opinion for the medical experts and save their precious time used in manual analysis. Magnetic resonance imaging (MRI) is the commonly used modality, as it produces detailed and fine contrast images of internal organs for diagnosis of PCa, but it may contain a certain amount of rician and gaussian noise which is necessary to be denoising before segmentation and classification. Denoising offers several challenges such as suppressing of significance image details leading in inaccurate segmentation and classification for prediction of abnormality. Thus, improved denoising, segmentation, and classification approaches can overcome the challenges by analyzing the pitfalls in the state of the art. This paper presents the experimental analysis state of the art denoising and segmentation approaches to analyse their performance based on the values of Peak signal to noise ratio (PSNR), Mean squared error (MSE), Structured similarity index (SSIM), dice metric, area overlap and accuracy. Based on the experimental analysis it was analysed that anisotropic filter outperforms other filters for gaussian noise with PSNR of 28.29, MSE of 96.22 and SSIM of 0.64. Also, for the rician noise anisotropic filter outperforms others with PSNR of 28.06, MSE of 101.52 and SSIM of 0.01. Similarly, for the combined gaussian and rician noise, anisotropic filter outperform others with PSNR of 28.34, MSE of 95.13 and SSIM of 0.652. Further, the analysis of segmentation approaches such as contour and shape-based, region/atlas based, thresholding based, clustering based and deep learning based was performed. Amongst these approaches deep learning based segmentation was found to outperform with dice metric of 0.89 and area overlap of 0.80. Also, CNN based classification outperformed machine learning based Support vector machine (SVM), K nearest neighbour (K-NN) and Random forest (RF) with 94.55% sensitivity, 93.34% specificity, 95.45% accuracy. Finally, the paper discusses challenges and future scope based on analysis in the concerned field for diagnosis of PCa.

Keywords PCa · MRI · Denoising · Segmentation · Classification

1 Introduction

Prostate Cancer (PCa) is a cancer that occurs in the prostate gland due to production of seminal fluid used to transport and nourish sperms. PCa [86] forms cells in the prostate gland present in men below the bladder in front of rectum as shown in Fig. 1, which increases in size with age due to rise in male hormone androgen. Prostate is a crucial part of male reproductive system, improper functioning of which could lead to drastic effects on excretion and reproduction phenomenon. PCa is a slow growing cancer and most of its cases cannot be predicted until it reaches an advanced stage. It actually hinders the functioning of semen production and urine filtration. Prostate cancer doesn't follow any particular symptom, most of the death cases are projected due to its irrelevant and awkward nature such as pain during urination, difficulty in bladder control, blood in urine and reduced flow of urine ejaculation etc. PCa may spread and form tumors leading to metastatic cancer with symptoms like swelling and pain in legs, hips or feet. These signs and symptoms are suggested ones but actual incidence of PCa can't be predicted with so much ease. It needs special care and awareness at certain stages before it becomes large enough to expand to other organs which is the most dangerous situation. Although various types of PCa occur in the prostate, most of them develop from glandular cells and other types are very rare. Recently, the American cancer society predicted that there will be around 161,360 new cases of prostate cancer by 2020, leading in 26,730 fatalities. Whereas, the actual incidence of PCa in Indians is quite lower than other western countries. According to the Cytecare Cancer Hospitals report [85], the 5-year survival rate for prostate cancer is 64%. PCa is one amongst the top ten cancers in India which generally occurs in old age i.e. more than 65 years but currently it has expanded its influence to youth as well. The cause for the same presented in literature includes obesity, improper diet and genetic changes. Also, the study at Mumbai revealed that the one who has gone through treatment or any surgery has better chances of survival. Although, it is good for medical analysis yet awareness and prevention of PCa has a significant role in enhancing survival rate. Projected cases of PCa in India are around 26,120 in 2010 and 28,079 in 2015.The study showed that it would be doubled by 2020 if left undiagnosed at an early state. Prostate cancer has become the second most occurring cancer in men after lung cancer [37]. Prostate delineation is a great challenge and everyday a new technology is brought up by scientists. Identification and medication of prostate diseases has become a cumbersome task for the experts. Prevention of PCa is not known in most cases as the cause of disease could not be defined

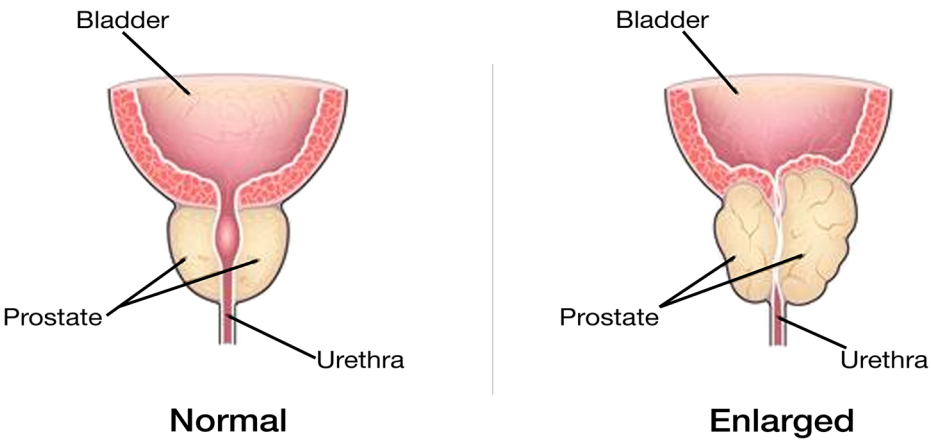

Fig. 1 Normal and abnormal prostate

accurately and precisely. But some common practices and measures could reduce the chances of its occurrence such as maintaining of body weight (avoid obesity), indulging into exercises, walking, running and eating a proper diet (green vegetables and fruits), avoiding the intake of processed and red meat and, reducing the intake of calcium rich dairy foods etc. These practices are common for many types of cancers besides PCa.

Being diagnosed with PCa is a life changing experience for the man as tedious therapies and treatments need complete commitment [10]. Commonly used procedures for investigation almost remain the same for all types of cancers. But treatment procedures may vary according to the patient's condition. For instance CADs [59] provides an intelligent, natural, and reliable way for the same. The goal of the CAD system is to be used as a second opinion for doctors and radiologists and, assist them to degrade biopsy rate, enhance the diagnosis accuracy and save their precious time. These systems use either CT, MRI or PET scans because each scan contains hundreds of images called slices that must be evaluated by a radiologist. Investigation of PCa consists of three-step phenomenon Detection, Diagnosis and Staging outlined in Fig. 2.

The prostate specific antigen blood test (PSA) and digital rectal exam (DRE) test can be used to detect PCa when no symptoms are observed. In the PSA test, level of PSA (a protein secreted by prostate gland) is measured whereas in DRE the expert inserts lubricated fingers (gloved) into the rectum to examine contortion in size and shape of the prostate. The detection is the preliminary step of almost all the types of cancer treatment. Its effectiveness decides the overall efficacy of the diagnosis. The detection procedure gives us the location, size, shape of cancer in the prostate and if performed at an earlier stage, can give better treatment options for PCa. After successful detection, diagnosis is performed by physicians to confirm the presence of disease. There is a significant role of imaging in primary diagnosis of PCa. The frequent analysis is performed by ultrasound and mp-MRI. Another procedure used is prostate biopsy which indicates the level of PSA. In some cases, prebiopsy would be required during diagnosis as it reduces the cumbersome procedure and painful treatment of biopsy. With the use of MRI modality, it would be concise, simple and less painful to diagnose PCa. MRI assists the experts to a great extent. Diagnosis with accurate results makes the classification of PCa easy. Further, the diagnosis includes classification and staging of tumors using advanced algorithms. Tumour classification separates out the level of tumours and provides a great assistance to physicians. However, many of the classifications are based on benign and malignant yet can be further categorized into T and N stages [11]. 'T' stage signifies the advanced stage of tumour which spreads to nearby tissues and 'N' stage signifies, if PCa has spread to lymph nodes or not. In some cases, stages could be analyzed by providing the ranks or some sort of numerics like stage 1, stage 2, stage 3 and stage 4 as shown in Fig. 3. Usually, Stage 1 is the early stage which is curable if diagnosed earlier, while stage 4 is the last stage and most fatal. Further, the number and type of staging could be decided based on the type and condition of the cancer. Also, the comfort and tolerance of patients are taken into consideration for suggesting the type of staging.

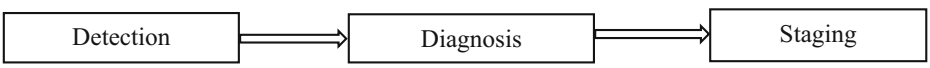

Fig. 2 Investigation methodology

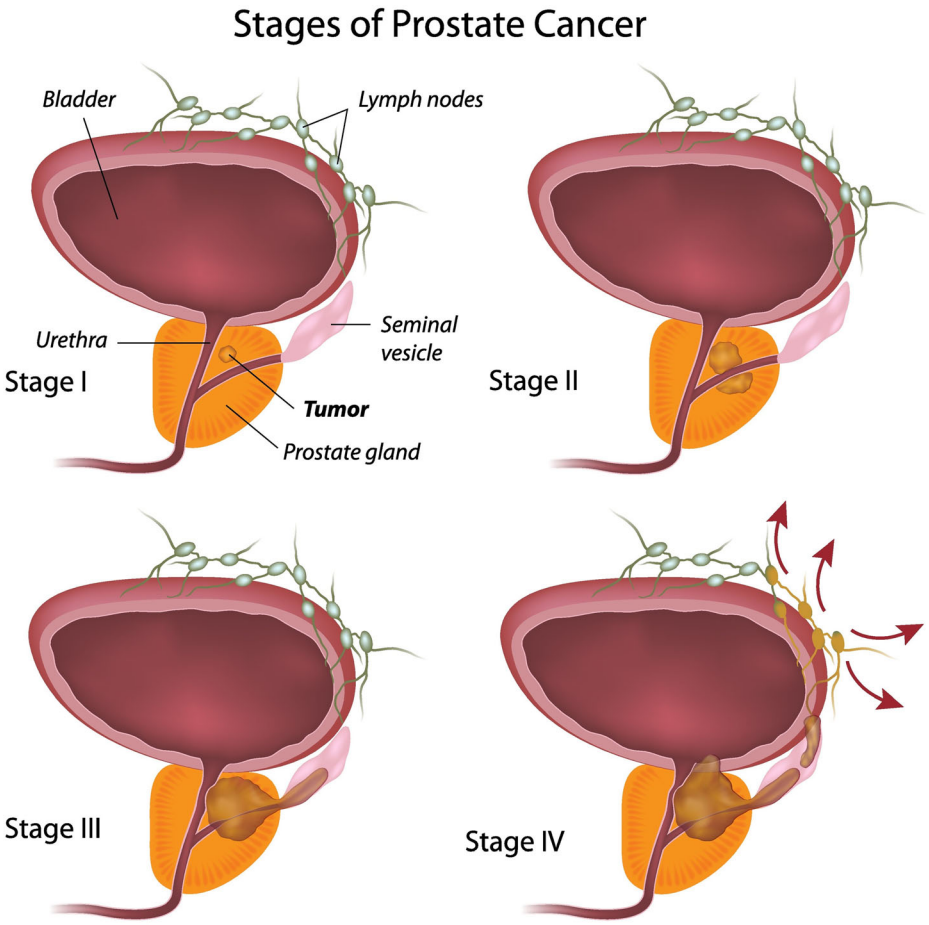

Fig. 3 Staging of Prostate

2 Imaging modality used for diagnosis

Different imaging modalities are used in the literature for diagnosis of PCa such as CT, MRI, mp-MRI, PET, Ultrasound, Radiomics etc. depending on the type and location of tumour [36]. Some of the commonly used imaging modalities are as follows.

2.1 CT [102]

Computed Tomography (CT) is a diagnostic test performed to take detailed images of internal organs, bones, soft tissues and blood vessels. The images acquired comprise multiple slices for further studies. CT scan uses the dose of ionizing radiation in patients for scanning which can cause serious threats to human health. CT is one of the painless and precise diagnostic medical investigations which use several x-ray projections to form a stack. CT scanning provides an additional benefit of curing any injury to internal organs by identifying the injured and affected part. Despite these benefits and applications, CT scan is considered less effective than MRI as the contrast detail is more in case of MRI. The need of X-rays during scanning makes the

process cumbersome and painful comparable to MRI. The advanced technologies make CT suppressive. It needs modifications and modern algorithms to cope up with the advancements. According to an estimation, 75 million CT exams were performed in the United States in the year 2009. Also, the studies suggested that 5% to 30% of total treatments, costs hundreds to thousands of dollars which is very high for developing countries like India. Figure 4 shows the CT scan of a patient with prostate cancer.

2.2 MRI [57]

Magnetic Resonance Imaging (MRI) scan uses strong magnetic fields and radio waves to get a detailed and fine image of internal organs with deformities. MRI is also a noninvasive painless procedure like CT, but does not use fatal x-ray radiations. MRI gives more detailed and contrast images of the anatomy which makes it easy for the physicians to find out any abnormality in the body with more accuracy than other imaging modalities. It uses radio frequency pulses to estimate and confirm the existence of tumour in the region of interest. MRI scanners are available with different magnetic field strengths ranging between 0.5 to 3.0 T, where 1.5 T is assumed as standard clinical setting. The quality of MRI scanning depends on the magnetic strength, here 1.5 T magnetic strength provides lower signal as compared to 3.0 T. It has been observed that 3.0 T can give unexpectedly perfect and bright images by performing scans in a small span of time, thereby decreasing the total scan time. According to the study conducted in Japan, there are around 48 machines for every 100,000 patients i.e. most MRI scanners per capita. Thus, it is considered to be better than other imaging modalities, also it does not involve any exposure to harmful ionizing radiations. MRI scanning can also produce mp-MRI images by different MRI sub-modalities like, dynamic contrast enhanced (DCE) MRI, Diffusion Weighted Imaging (DWI), T1-weighted and T2-weighted etc. Figure 5 given below shows the MRI of prostate cancer.

2.3 Multiparametric MRI (mp-MRI) [4, 38]

Multiparametric MRI is much more famous than usual MRI due to the involvement of multiple parameters in imaging. mp-MRI is an emerging modality that has been added to PSA based

Fig. 4 CT scan of prostate cancer [27]

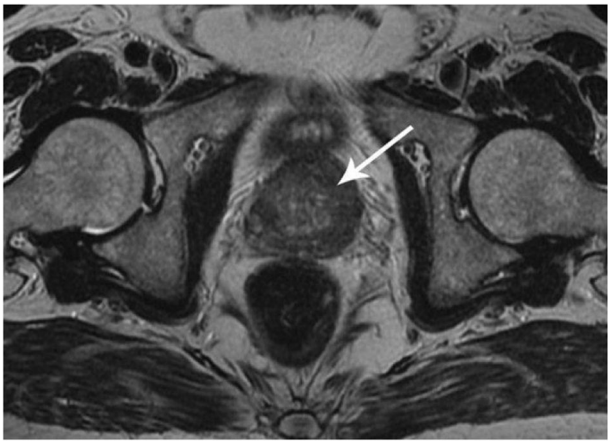

Fig. 5 MRI scan of prostate cancer [95]

PCa screening to improve the diagnosis, complexity of therapies and management of cancer. mp-MRI is a functional form of imaging technique essentially used to improve conventional anatomical T1 and T2-weighted imaging. It also enhances the efficacy of diffusion-weighted imaging (DWI) and dynamic contrast enhanced (DCE). Recently, an advanced technique MR spectroscopy has come in favor of mp-MRI. However, spectroscopy is not an easy process to be implemented as it requires post processing and inputs from the medical experts to make it less effective than standard MRI examination. Collaboration of mp-MRI with other biopsies could be an efficient way of treatment. Mp-MRI followed by TRUS biopsy reduced the unnecessary diagnosis when compared with common mp-MRI. Mp-MRI is observed to be more sensitive and less specific than TRUS biopsy. Fig. 6 shows the mp-MRI of prostate.

2.4 PET [28]

Positron emission tomography (PET) involves the imaging of internal organs with the help of certain radiotracers. Fusion of PET with computed tomography (CT) and Magnetic Resonance Imaging (MRI) are frequently used in the treatment of PCa. Positron emission tomography/

Fig. 6 mp-MRI -Prostate cancer [7]

computed tomography (*PET*/CT) has recently emerged as a promising diagnostic imaging platform for prostate cancer. Currently, choline PET/CT has been the most extensively studied modality which uses 18F-fluorodeoxyglucose (FDG), a workhorse radiopharmaceutical in PET and does not find preference in PCa since these tumors show poor glucose uptake. Likewise, there are many more radiotracers which are being used in PET according to the requirements of treatment techniques. PET constitutes the challenge of true sensitivity and specificity. The implications of metastatic findings on primary and recurrent staging need to be explored more and more. Enhanced PET quantification opened many avenues for clinical diagnosis, assessment of response to treatment and therapy planning. Conventional imaging modalities are very poor in finding the extent of disease in the case of biochemical recurrence. PET has advanced utility to deal with biochemical recurrence. PET Radiomics in non-small cell lung cancer (NSCLC) make it more effective. Thus, response assessment and prediction are one of the reasons discussed for using PET in Radiomics. Figure 7 shows the PET image of the prostate.

2.5 Radiomics based [40]

Radiomics is an approach to extract a large number of quantitative features from medical images using some data characterization algorithms. Radiomic features (features extracted) have the ability to extricate hidden disease characteristics. Radiomics is a field of cancer treatment and management which uses advanced imaging methods to extract a number of quantitative features. It involves many of the application areas of radiomics like prediction of treatment response and outcomes, tumour staging, tissue identification and assessment of cancer genetics. Recently, radiomics is getting fused with machine learning methods to surplus the quality of results which is increasing with speed. Radiomics has the potential power to hasten better clinical decision making. The mining of radiomics based features for some sort of correlations with patterns invented other sub modalities like radiogenomics, pyradiomics etc. Pyradiomics reduces the issue of radiomics standardization which is derived from phenotypes that can be linked to genomics data referred as “radiogenomics”. Radiomics provide an open

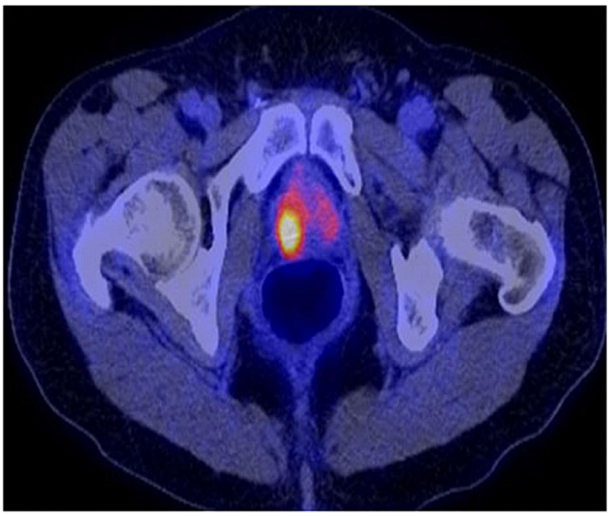

Fig. 7 PET-Prostate cancer [19]

source platform for engineering of large-scale feature extraction with suitable reproducibility and 3d tumour volume delineation. Figure 8 shows the steps of radiomics and radio genomics of PCa.

Some of the common differences among the above discussed modalities are explained in Table 1.

Based on the comparison of different imaging modalities, it can be analysed that MRI is a commonly used and best imaging modality for diagnosis of PCa as it does not involve any kind of harmful ionizing radiation as in the case of CT, ultrasound and X-ray imaging modalities. Moreover, contrast details of soft tissues, highlighted images of blood vessels are some of the specialized features of MRI which makes it better than other imaging modalities. Speed of scanners leading in improvement of accuracy has been enhanced upto a level to give better results for MRI.

MRI before biopsy is considered an essential detection technique for any part of the body. In most of the cases, it is performed after a biased decision in initial testing of disease to confirm the patient's abnormality. An MRI scan can detect any deformity in the body by going through the contrast detailed images of the expected regions and body parts. Use of MRI has also increased the ability of physicians to provide complete routine studies in approximately ten to fifteen minutes to a large number of patients at the same time. Further, the increased quality of machines provides precise results at the end of the experts to perform rest of the procedures efficiently [12]. Thus, there is less probability to replace MRI with other imaging

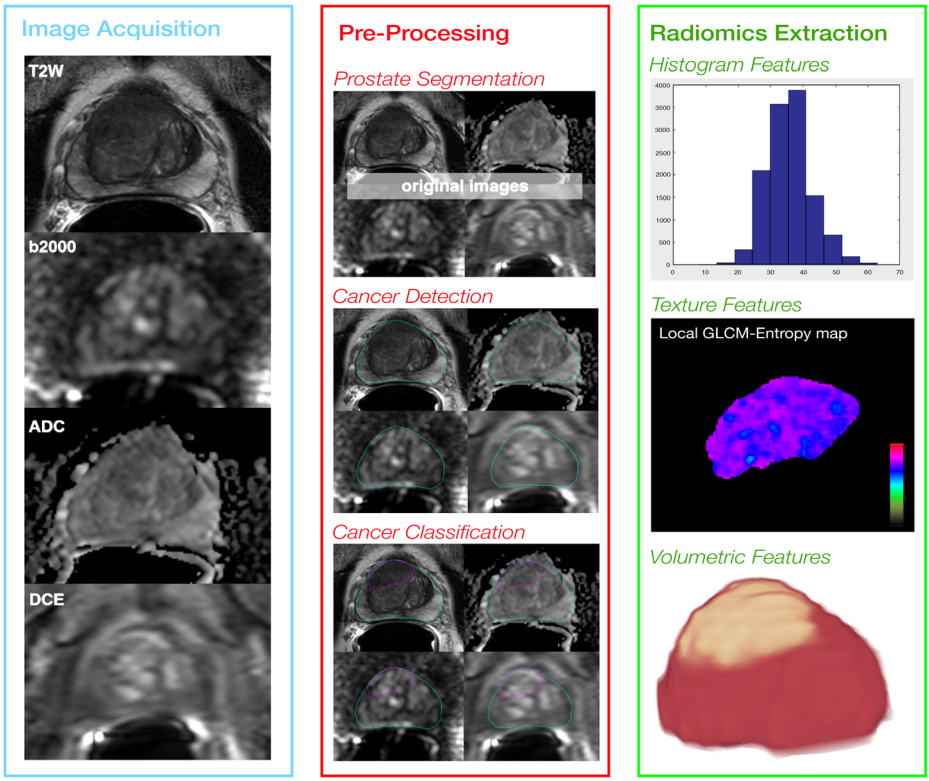

Fig. 8 Radiomics and radio genomics of prostate cancer [101]

Table 1 Comparison of Different Modalities

MODALITY	CLINICAL USAGE	ADVANTAGES	DISADVANTAGES	FUTURE PROSPECTS
CT [97]	Determining seed location during prostate brachythera-py.	Beneficial in calculating the extent of PCa to bone tissue.	Challenging for implementing real time imaging	Lesion Detection, cancer staging
MRI [39]	Exquisite soft tissue contrast, treatment planning, musculoskele-tal neoplasms	No exposure to harmful ionizing radiations, excellent contrast detail creates detailed images of blood vessels, much faster and simple to operate	High cost associated, Accessibility problem for specific protocols clinical institutions	Cost, time and Reproducibility of the advanced protocols making it feasible for use as a screening tool.
mp-MRI [39]	Initial diagnosis and recurrence, active surveillance, staging.	Excellent tissue contrast for identification of clinically significant PCa	Expensive due to in-bore time, lack of real-time imaging, requires advanced training	Alternative inbore options with real time imaging being developed
PET [18]	Staging, recurrence, metastatic spread	Offers ancillary information for tumor staging, characterization and metastatic involvement	Expensive, technological (e.g. attenuation correction) and/or clinical challenges (e.g. radiation ex-posure)	Development of specific radionuclides is an ongoing endeavor
Radiomics-based [80]	Extraction of large number of quantitative features from medical images	Tumor Staging, prediction of treatment	Reproducibility and computation of radiomic features	Machine learning in automation of data characterization algorithms

modality for diagnosis, as it has reached a very high level of diagnostic significance and is thus preferred.

3 MRI public datasets

Recently, for the diagnosis of PCa many datasets have been made publicly available in different formats such as images, text etc. The use of these datasets is strictly dependent on the situation of the problem. Two significant imaging datasets commonly used are as follows:

3.1 Prostate -benchmark dataset[1]

This dataset is publicly available since 2015 solely for the research purpose. It constitutes mp-MRI data collected from two significant commercial scanners, first one is 1.5 T general electric

[1] https://i2cvb.github.io/#prostate-data

(GE) and second one is 3.0 T Siemens scanner. The images in the dataset are mainly available in DICOM (.dcm) format. Various sub-modalities of MRI such as T2w, DCE, DWI and Magnetic Resonance Spectroscopic Imaging (MRSI) are acquired using different settings of scanners. Moreover, some evaluation parameters are also discussed for diagnosis purposes. Apparent diffusion coefficient (ADC) maps are provided in the data acquired with Siemens scanner. In the dataset each modality comprises a certain set of ground-truth values. The ground-truth contains four different classes: (i) prostate gland, (ii) peripheral zone (PZ), (iii) central gland (CG), (iv) CaP. These classes make the dataset more effective for developing computer aided detection systems. Till date, there is no such publicly available dataset with all these four individual classes for ground-truth. For each of T2w, DCE and DWI, 300 images of mp-MRI are provided in the dataset. Most of the filters have been implemented till date on this dataset and testing of new filters are also being carried out by the researchers across the globe [64].

3.2 Prostate – MRI[2]

The dataset has been made public for use since 2016. This collection comprises 22,036 images. Prostate MRI is acquired with an endorectal and phased array surface coil at 3 T (Philips Achieva). The main imaging modality used in the dataset is MRI with a few PET/CT additional data collection. The dataset comprises 182 images from 26 patients, where each patient had gone through biopsy and had confirmed the PCa. Patients examined in the dataset have also undergone a robotic assisted radical prostatectomy. A mold was developed from each MRI and the prostatectomy sample was taken in the mold to cut the same plane as the MRI. The data was produced at the National Cancer Institute, Bethesda, Maryland, USA between 2008 and 2010 [25].

4 Literature survey

4.1 Denoising

Denoising is the initial step of the CAD system which plays a major role in performance of segmentation and classification. Many internal and external factors contribute in increasing the noise level of an image leading in the development of different optimized image denoising algorithms. Although MRI scanning techniques had effective results in signal-to-noise ratio (SNR) acquisition speed and spatial resolution. The noise was produced during the procurement process due to varied sources such as physiological processes, eddy currents, magnetic susceptibilities, body motions etc. Denoising is necessary for accurate results in order to map the structural and functional aspects of human anatomy [90, 119]. Common noises in MRI are rician noise and gaussian noise. Rician noise is a single-dependent noise following rician distribution making it difficult to separate from signals at low SNR regimes. It hampers image analysis by worsening MR images quantitatively and qualitatively [9]. Whereas, gaussian noise consists of normal distribution and identical probability density function (PDF). The divergence values could be taken by the noise on being gaussian distributed making it gaussian noise [74].

The denoising filters used by different researchers for MRI are as follows:

[2] https://wiki.cancerimagingarchive.net/display/Public/PROSTATE-MRI

A low pass filter named **Median filter** mollifies the unpredictable noise via a non-linear process. It smoothens the image by substituting the central pixel with the equivalent median of these pixels subsiding beneath the mask. The dimensions of the edge are of n/2 x m/2 size, with nxm being the size of window mask is also eliminated with this filter leading to a fuzzy image. While for a window mask of the dimensions n x m, every pixel's median value is centered along the axes as (i, j), sorted in increasing order to get a new value for the pixel (i, j) [52]. Later, Sazanita Isa et al. in 2015 proposed three varied algorithms as adaptive filter (ADF), average filter (AVF) and median filter (MF) to denoise the MRI images. To increase the performance of the filters, the noise density was increased upto 90%. The peak signal to noise ratio (PSNR) and mean squared error (MSE) added to the efficiency of the filters. This filter gave a better image than other prescribed filters used in the literature [55]. Recently, Hanafy et al. in 2018 proposed a modification in median filter algorithm. The MRI image having salt, pepper and gaussian noise alternatively called impulse noise was passed through median filter, adaptive median filter and adaptive wiener filter. The performance measure of different filters was evaluated and exploited against the PSNR. De-noising of the original image was challenging as it caused blurring with addition of artifacts. The quality of the image got defective while capturing, processing and storing it. While in clinical diagnosis, the high-quality images were affected by different types of noise. Further to reduce it, the challenge was to regularize the image while conserving the details. The MRI denoising filters were described in the dimensional, transformed domain and exploitation of the statistical properties of signals. Thus, the filtering reduced the noise and was responsible for the interpolation and resampling. The adaptive Wiener filter used a pixel wise statistical approach using neighborhoods of m x n size, to filter the image. The non-linear filters performed a notch higher than the linear filters and smoothened the images by reducing the intensity variations between the pixels. It was commonly used in signal processing and time series processing. Thus, the high intensity impulse noise was filtered using above approaches and the adaptive median filter was found to outperform other filters [6].

Wiener filter uses the least mean square (LMS) method to reduce the disparity between the preferred and filtered output. The filter coefficients are adjusted and minimized according to the disparity. By inverting the discrete fourier transform (DFT), a final resultant is achieved and hence the noise process, power spectrum of signal and the wiener filter is defined [23]. Also, J. Mohan in 2013 presented a new filtering method for the magnetic resonance images (MRI) to remove rician noise based on nonlocal neutrosophic set (NLNS) Wiener filtering. Neutrosophic set (NS) studied various interactions with the ideational spectra applied into the image domain and performed denoising. The MRI image was passed through the nonlocal mean and converted into NS domain with three values indeterminacy (I), false (F) and true (T). Further, its entropy was defined to measure the indeterminacy. The clinical images from the Brainweb database were denoised using the w-wiener filter that produced better results than the other classical methods [79]. Biswas et al. in 2017 proposed a method for denoising of brain MRI using curvelet transform with addition of the wiener filter. The images were distorted with various noises from the environment during acquisition, storage and transmission of the dataset. This hybrid approach was compared with curvelet and wavelet-based technique and was more effective than the latter in performance and efficiency. Further mean square error (MSE), structural similarity index measure (SSIM) and PSNR were calculated to completely denoise the image [15].

Gaussian filter is a blur removing convolution filter to handle noise with an equivalent filter generated by the neurons. Its application is a two-way process where the gaussian distributed weighted mask is convolved to filter the image pixels in order to obtain the new pixels. Firstly, it is carried out horizontally and then vertically, if the window size is large there are high levels of blurring and vice-a-versa. This filter eliminates gaussian noise upto a great extent by blurring the

edges and the gaussian function defined in both the dimensions [68]. Also, Roth and Black et al. in 2005 proposed a field of expert (FOE) model that consisted of computations with upper bound for training along with the learning of the non-innate potentials. The log partition was tightly bounded on the lower and upper bounds to get a basis rotation algorithm. The Gaussian potentials were used in the machine learning algorithms [93]. Thereafter, Weiss and Freeman in 2007 applied the Gaussian Scale Mixture (GSM) process for the FOE model before the use of legitimate images [114]. Later, Barbu in 2009 used the suboptimal inference process to train Conditional Random Field (CRF)/ Markov Random Field (MRF) that was based on the bayesian framework merged to train an active random field (ARF) with optimized loss function for a pair of input images and resultants. The images were denoised using collaboration of FOE and MRF [13]. Thereafter, Seetha J in 2016 performed denoising of MRI using filters namely gaussian and median based on commonly used criteria such as energy, contrast, entropy, PSNR, correlation and variance [98]. Similarly, Liu et al. in 2019 proposed an image restoration model that used maximum a posteriori (MAP) estimation on the imaging dataset of MRI. Rician noise and intensity nonuniformity present in these images were denoised using an optimization algorithm based on ADMM. It divided the problem into various subproblems that were solved by either closed-form solutions or Newton's method. The intensity divergence actually underestimated the noise and so was better to handle the rician noise. Earlier these noises were individually dealt with, however the MAP estimator regarded MRI data as amalgamation of dual multiplicative components, the real identity, the bias field and the rician noise. The calculations and experiments performed on this method using real and synthetic MR datasets confirmed its efficiency as compared to other methods in the literature [72].

Mean filter substitutes each pixel with a mean value of the pixels through a convolution process to reduce the level of intensity deviation between two successive pixels. The neighboring pixel values are not taken into account, hence smoothens the overall image. For a larger window size, the noise is removed significantly adding onto the blurring effects simultaneously [48]. In the same year, Buades et al. in 2005 devised the Non-Local Means filter utilizing the redundant image information. Here, the pixel value was given as the output to calculate the mean of all the intensities of pixels in an image. This algorithm was quite complex wherein the family of weights relied on the closeness between the pixels i and j. These pixels were measured as a non-increasing function of the weighted euclidean distance between two pixels [16]. With few modifications, Fernandez et al. in 2008 devised the linear minimum mean square error (LMMSE). This method was adopted for the rician distribution and the noise power was estimated automatically. It restored the image by suppressing the noise with easy implementation and feasible computation cost [5]. Further, Luisier et al. in 2012 proposed the chi-square unbiased risk estimation (CURE). The recommended method could remove the noise from the squared-magnitude MR images. Linear expansion of thresholds (LET) were also familiarized which were executed on the filter bank transform coefficients. The wavelet transform was the inference of the dependent CURE approach [73]. Also, Rajan et al. in 2012 recommended that from the total methods proposed for image denoising, only some procedures could estimate the real characteristics of the MR images that achieved phased-array coils. The data collected from these phased-array coils were transformed into the root sum of squares in an environment free of noise correlations by following a non-central x distribution. The noise level became dimensionally fluctuating in intensity due to an increase in the acquisition speed of subsampling in the k-space of the GRAPPA method. The non-central–x distribution and the spatial essence of the noise was removed using multiple-coil acquired MR images [87]. In the same year, Gloshan et al. in 2013 recommended an LMMSE based strategy for the 3-D MRI denoising technique. The inefficiency of the LMMSE method estimated the noise less signals and the fact that the 3-D images contain samples to improve the estimation that made the approach to change a bit. The MR data was

modelled as random fields and the samples were chosen from a large portion of the given dataset. Based on the statistical moments of the image, the effective similarity measure was present and the local signal-to-noise ratio chose the filters and the approach to recursively denoise the image while safeguarding the anatomy of the image [41]. Further, Sudeep et al. in 2015 initiated the four filters for denoising that relied on the linear minimum mean square error (LMMSE) estimation. The performance was increased using natural redundancy and self-similarity techniques in the MRI imaging using the best samples for the LMMSE estimation. The uncorrelated noise was removed using the non-local PCA domain shrinkage. The Rician LMMSE enhanced the magnitude of the images by estimating a closed form systematic elucidation to the inverse problem. The filtering was done sub optimally as it could not take privilege of the data redundancy. The nonlocal implementation was done via LMMSE estimation method and the euclidean distance was computed by similarity weights in the spatial or transformed domain. This filter decreased the signal reliant fundamental unit of the noise but the remaining white part was filtered via second stage LMMSE filtering in the PCA (Principal component analysis) domain. Hence the given filters surpassed the performance given by the state-of-the-art methods [104]. Similarly, Manjon et al. in 2015 proposed an MRI denoising technique that took the advantage of both the self-similarity properties and sparseness of the MRI imaging. The local PCA allowed the sparse representation compared to local DCT. The dual stage proposal filtered the image having noise with a nonlocal PCA thresholding strategy which checked the elevation in the noisy image automatically. The other approach used this filtered image within a rotationally invariant non-local means filter to correct the rician noise induced locally. The comparisons made with the prescribed state-of-the-art methods revealed its efficiency [76]. Further, Klosowski J in 2017 proposed a denoising filter for real-time MRI. The small details were preserved while removing the framework noise without any smearing, patch or blur artifacts. The comprehensive conservation of the image was enhanced by a weighting kernel that roughly gave the exponential weight and removed the background noise. The filter used signal-to-ratio (SNR) to at least 60% while preserving the details. There was a straightforward estimation to a number greater than 100 complex frames per second via graphics processing units [60]. Also, Yuan et al. in 2018 proposed an improved variational level set method to remove the noise from the MRI degraded using rician noise. The automatic assessment of the standard deviation of rician noise gave more robust outputs. The fluctuating course method of multipliers ADMM was used along with this approach to increase its performance and capability [116]. More recently, Sharma et al. in 2019 gave the concept of sylvester-lyapunov equation and non-local means method as the old used filters did not give the desirable results. The denoising techniques retained and amplified the diagnostic related information of the images. The hybrid denoising techniques were contrasted with the other filters in the literature by changing the noise levels in the dataset of brain images and the real approach used PSNR, SSIM coefficients to calculate efficiency [100].

Wavelet filter uses energy compaction features to denoise the images suffering from gaussian noise. An input and noisy signal includes noise of salt, pepper, speckle or gaussians, which undergoes a wavelet transform succeeded by an inverse wavelet transform. While transforming, the noise is homogeneously distributed throughout the coefficients, but the large coefficients have the maximum information. At times, the selected threshold may not be applicable for the apt distribution of signal components of the noise at different proportions. Discrete Wavelet Transform (DWT) characterizes the features spectrally and removes out maximum noise keeping the necessary information. Its demerits are that it lacks adaptivity, phase information and is computationally expensive. The shifts in signal results in wavelet uncertainty coefficients. These filters can be used in quantum mechanics, fingerprint verification, speech recognition, signal

processing and related fields [43]. Cands and Donoho in 1999 proposed the curvelet transform model using multiscale geometric analysis. The anisotropy and directionality detected the edge directions with the small number of coefficients to handle the curve discontinuities. In the denoising process, curvelet threshold norms were calculated and the noisy image was transformed using a curvelet filter. Finally, the image was denoised by the application of the hard thresholding to obtain curvelet coefficients succeeded by the inverse curvelet transform [20]. After a few years, Romberg et al. in 2001 gave the nine meta-parameters in the Hidden Markov Tree (HMT) model. These were fixed using Bayesian universal HMT (Uhmt) independent of the number of wavelet scales and image size. It could be used in real life as it was quite simple and did not require any training. The structure of the image was integrated into a smart wavelet shrinkage rule using a bayesian methodology and the prediction helped to minimize the noise [92]. Further, Do and Vetterli in 2005 laid the foundation of a contourlet filter which captured the contours and other details of the image. The two distinguishing and subsequent decomposition phases in multiple scales, directions characterized the texture features and contours of an image. The contourlet transformations were used to perform the multiscale decomposition followed by calculation of scales and the number of directions with thresholding applying on them. The inverse transform on the contourlet coefficients reconstructed the image free of noise [29]. Similarly, Bhadauria et al. in 2013 recommended a denoising method for magnetic resonance imaging (MRI). Due to the acquisition of images from different machines, the medical images contain various noises that hamper the required information in the images. The proposed method blended the denoised images using total variation (TV) method, edge formation and curvelet method. The noise residual of the TV method provided the edge information that was processed using a curvelet transform. The efficiency of this approach was depicted in edge preservation and noise suppression [14].

The **bilateral filter**, a non-linear filtering process decomposes an image into a variety of proportions after the required changes with no creation of aureoles. It is therefore used in denoising and many computational photography applications such as relighting. Its working is similar to the gaussian convolution and is reliant on the two inputs as the size and contrast of the features. The calculations include mean weights of the neighboring pixels along with value difference to detect the edge information while smoothening [17].

Perona and Malik et al. in 1990 gave **anisotropic diffusion filter** to maintain the object periphery while raising the image quality. The edge sharpening reduced the noise in uniform regions and the non-linear diffusion scheme was used to localize the linear diffusion filtering and avoid blurring. The problem was determined in the form of a second order partial differential equation of heat. The places having higher probability to be edges were located and diffusivity was diminished therein [84].

Finally, Table 2 presents the summary of all the denoising approaches used by different researchers from time to time as discussed above and Table 3 presents the comparison of broadly used state of the art denoising approaches with pros and cons of each approach.

4.2 Segmentation

This section presents the approaches used by different researchers for segmentation of prostate. The approaches used are broadly categorized into six modules i.e. Contour and shape based, Region/Atlas based, Thresholding, Clustering, Deep learning and Hybrid.

Table 2 Summary of Denoising Approaches

Authors	Year	Approach	Pros	Cons
Cands et al. [20]	1999	Curvelet transform model	Visually lossless	Creates problem in formation of curvelets on smooth areas
Romberg et al. [92]	2001	Hidden Markov Tree model	Supported the prediction of wavelet coefficient, Independent of image size	Works only on horizontal, vertical and diagonal edges
Do and Vetterli [29]	2005	Contourlet filter	High directionality, adjustable aspect ratio	High computations
Buades et al. [16]	2005	Non-Local Means filter	Conserves the originality of image	Intricates weight calculations
Roth and Black [93]	2005	Log partition	Used for gaussian noise	Only suitable for specific noise
Weiss and Freeman [114]	2007	Gaussian scale mixture process	Sampling is not required	Handles small amount of noise only
Fernandez et al. [5]	2008	Linear minimum mean square error	Feasible computation cost	Suppress image details along with noise
Barbu [13]	2009	Markov random field/ Conditional random field	High accuracy and speed	Works well with higher number of parameters
Luisier et al. [73]	2012	Chi-square unbiased risk estimation	Flexible computation	Suppress image details
Rajan et al. [87]	2012	GRAPPA method	Removes spatial noise	Complex computation
Bhadauria et al. [14]	2013	Total variational method, curvelet method	Preserves edge	Modifies smooth areas
Gloshan et al. [41]	2013	LMMSE-based strategy	Recursive noise removal with preservation of anatomy	Inefficient for high noise signals
J. Mohan [79]	2013	Nonlocal neutrosophic set wiener filtering	Removes rician noise	Filters only in non-local means
Sazanita Isa et al. [55]	2015	Median filter, adaptive filter and average filter	MSE and PSNR increase the efficiency	Increased noise density
Sudeep et al. [104]	2015	Linear minimum mean square error estimation	Self-similarity and natural redundancy	Does not use redundant data
Manjon et al. [76]	2015	Nonlocal PCA thresholding	Self-similarity and natural redundancy	Requires complex staging approach
Seetha J. [98]	2016	Median and gaussian filters	Increased efficiency	Computationally expensive
Klosowki J [60]	2017	Weighting kernel and graphics processing units	Improved SNR, Straightforward computations	Approximation of exponential weight
Biswas et al. [15]	2017	Curvelet transform with addition of the wiener filter	Improved performance	Inverse filtering and noise smoothing
Hanafy et al. [6]	2018	Median filter, adaptive median filter and adaptive wiener filter	Impulse noise removal	Costly and complex to computation
Yuan et al. [116]	2018	Variational level set method and alternating direction	Image gradient retains edge details	Does not eliminate heterogenous noise

Table 2 (continued)

Authors	Year	Approach	Pros	Cons
		method of multipliers		
Sharma et al. [100]	2019	Sylvester lyapunov equation and non-local means method	Improved performance	Complex in computation.
Liu et al. [72]	2019	Maximum a posteriori estimation	Combination of two multiplicative components	Intensity nonuniformity miscalculate the results

4.2.1 Contour and shape based approaches

These approaches are based on the appearance of objects and rely primarily on their shape. It considers bounding contours as cue for detection of objects, which includes approaches such as active contour, active shape model etc. for extraction of desired region of interest [66]. Some of the approaches used by researchers for segmentation of prostate using contour and shape based are as follows:

Samiee et al. in 2006, presented a semi-automatic segmentation algorithm based on the orientation property which is intrinsic to the prostate MRI used in evaluating the direction of tracing curves. On evaluating the algorithm on 2 MRI volumes with 19 slices each, the proposed algorithm yielded an average DSC values of 0.8856 with 0.0041 variance of the dataset with the deflated endorectal coil and the one with inflated endorectal coil yielding an average DSC of 0.9057 with 0.0014 variance. The segmentation process took no more than 5 s using MATLAB and an intel Pentium 4, 2.8 GHz PC platform [96]. Thereafter, in 2007 Zhu et al. proposed a hybrid methodology including both 2D and 3D Active shape models (ASM) to deal with sparse 3D data. Rather than aiming at the segmentation of local optimum on separate slices, the proposed paradigm aimed at segmenting a global optimum of the 3D object. The dataset for evaluation contained 26 MRI sequences with a total of 288 slices containing the prostate gland. The proposed algorithm indicated a high precision value as compared to 2D and pure 3D ASM by yielding the lowest RMSD mean and standard deviation values of 5.4811 and 2.9082 respectively [118]. Further, Flores-Tapia et al. in 2008, developed

Table 3 Comparison of Denoising approaches

S.No.	Approach used	Pros	Cons
1	Median filter	Non linear nature of this filter preserve sharp details	It is difficult to treat the analytical effect of this filter.
2	Wiener filter	Offers perfect reconstruction	Requires prior knowledge of image without noise.
3	Gaussian filter	Perform effective smoothing	May lose significant edge details
4	Mean filter	Smoothens the image	May lose significant edge details
5	Wavelet filter	Efficient reconstruction and computationally less expensive	Produce blurring effect
6	Bilateral filter	Preserves edges	Causes Gradient distortion
7	Anisotropic filter	It reduces noise in flat regions as well preserving significant edge details	May reduce image resolution

a novel paradigm for MRI prostate image segmentation. In order to accurately detect the borders around the prostate, the proposed method exploited the disparate behavior presented by noise in the wavelet domain and signal singularities. The prior knowledge about the general shape of the prostate and set of spatially variant rules were utilized to trace the prostate contour. The performance of the proposed method was assessed by applying the algorithm to a pelvic MRI volume formed by 19 slices. The mean DSC value for the processed data was observed to be $0.93 \pm .005$ [32].

Thereafter, in 2010 Gao et al. proposed a unified shape-based paradigm to extract the prostate from MRI. The proposed algorithm represented the shapes of a training set as point clouds in order to solve the registration problem by exploiting additional global aspects of registration by the virtue of a particle filtering based scheme. Additionally, once the shapes were registered, a cost function was designed to incorporate both the local image statistics as well as the learnt shape prior. The proposed method performed better with the running time of 2.3 s when compared with MSE and MI with run time being 433.5 s and 610.0 s respectively. The segmentation results were validated employing 33 MRI prostate data yielding mean DSC of 0.84 with standard deviation of 0.03, 95% of HD and (8.10, 1.50) standard deviation [34]. In 2011, Liu et al. gave an unsupervised paradigm employing shape-based active contour model without needing the training data for segmentation. The segmentation was performed on 3D apparent diffusion coefficient (ADC) images derived from diffusion-weighted imaging (DWI) MRI. The algorithm estimated the shape of the prostate by applying course segmentation using a region-based active contour model for 3D ADC images to perform segmentation with shape priors. After the additional surface refinement, the segmented prostate volume was generated. The algorithm was evaluated on 10 patients yielding DSC of 0.810 ± 0.050, mean absolute distance (MAD) of 2.67 ± 0.650 mm and HD of 9.07 ± 1.64 mm for the whole prostate gland [21]. After that in 2012, Malmberg et al. proposed a generic tool for interactive image segmentation using smart paint. Transversal T2-weighted MRI was used for the evaluation of the proposed method. The proposed segmentation tool worked on the principle of user adding or removing details in 3D and the user interface displaying the segmentation result in 2D slices through the object. To quantitatively measure the difference between obtained segmentations and the ground truth, dice's coefficient was used. The segmentation using this method took 2 rounds for segmenting the training set and the mean dice coefficient for the first and second rounds were 0.82 and 0.86 respectively. It took 3 min and 30 s on an average to segment a volume in the training set and 4 min 44 s for the testing set [75]. Similarly, Chandra et al. in 2012 presented a novel paradigm to automatically segment the prostate and its seminal vesicles. The proposed deformable model was case specific and consisted of an individual patient's initialized triangulated surface and image feature model. The presented segmentation algorithm consisted of regularizing the deformations produced by employing the image feature model via surface smoothing algorithms which was then automatically validated by the virtue of an optimized shape model. The proposed method produced a mean and median DSC of 0.85 and 0.87 with 3 T MR clinical scans of 50 patients used for validation. The median DSC result had a mean absolute surface error of 1.85 mm [22]. Later in 2014, Guo et al. presented a new deformable, nonparametric appearance paradigm for prostate segmentation in MRI. The proposed model was based on a novel learning method incorporating distributed discriminative dictionary (DDD) learning. The learning method used was able to capture precise distinctions in image appearance. The proposed method aimed to robustly segment the prostate gland in 3D T2-weighted MRI images by using both appearance and sparse shape models to derive a deformable model for segmentation. For the first internal dataset, the proposed method yielded a DSC of 0.891 and for the second dataset which was the MICCAI 2012 challenge dataset, the proposed method yielded a DSC of 0.874, which also achieved improved segmentation accuracy

than other methods under comparison [46]. Further in 2015, Tian et al. presented a "Supervoxel" based method for prostate segmentation. The proposed paradigm employed an energy function and smoothness terms to model the labeling process. The smoothness term was constructed taking into account the geometric relationship between two adjacent supervoxel and the data term to estimate the probability of a supervoxel according to the shape feature. The experimental results achieved by the algorithm on 12 prostate volumes with mean dice similarity coefficient of 86.9% ± 3.2% suggested the competence of the graph cuts algorithm for handling large three dimensional (3D) medical data. The presented algorithm yielded a smooth surface based on the output of the 3D graph cut by utilizing a level set in order to segment the prostate [105]. With few modifications, He et al. in 2017 gave a robust, fully automatic prostate segmentation method based on active shape model. The presented model employed a novel adaptive feature learning probability boosting tree (AFL-PBT) for initialization, and deep learning techniques were utilized to re-extract features. Also, in order to enhance the optimal boundary, a narrow searching band utilizing the PBT map was used. The algorithm when tested on MICCAI PROMISE12 test data sets produced a mean DSC of 84% with a standard deviation of 4%. On contrary to the traditional ASM method, the proposed model had the entire proposed framework insensitive to model initialization. Also, the model employed a CNN based deep learning design for boundary profile modeling. The use of a relatively simple CNN model and 2 level probability boosting tree served as the agents limiting the accuracy of the proposed method [50]. In the same year 2017, Guo et al. proposed a novel deformable prostate segmentation method for MRI. The presented algorithm integrated the deep feature learning with the sparse patch matching and was broadly evaluated on the dataset comprising 66 T2-weighted prostate MRI. To incorporate more succinct and effective learned features than the handcrafted features, the proposed method employed the stacked sparse auto-encoder (SSAE) to learn the latent features from the MRI and used a sparse patch matching method to deduce a prostate likelihood map. Finally, the integration of the sparse shape model and the likelihood map was achieved by employing the deformable segmentation. The proposed supervised SSAE with deformable model achieved DSC of 87.8 ± 4.0, precision of 91.6 ± 6.5, hausdorff of 7.43 ± 2.82 mm and ASD of 1.59 ± 0.51 outperforming the ASM, the intensity based deformable model, and the handcrafted based deformable model with deviations of 10.7%, 2.1% and 1.6%, respectively [47].

4.2.2 Region/atlas based approaches

These approaches use pre-labeled images, called atlas or initial seed to segment the image with user involvement. The approach uses three phases, firstly to align objective image with multiple or single images/seeds, thereafter relocation to target from atlas/seed to objective image and finally, delineation to relocate labels applied to extract the target image [91]. Studies performed by different researchers for segmentation of prostate using region/ atlas-based approach are as follows:

Initially, in 2010 Martin et al. proposed a fully automatic paradigm for the segmentation of the prostate in 3D magnetic resonance images. The proposed method registered a target image (to be segmented) to a labeled image (atlas). The encompassed deformable model substantially refined the segmentation obtained using the atlas by reducing the mean errors from 3.14 to 2.41 mm. The proposed segmentation algorithm incorporates two stages. A probabilistic segmentation was obtained by tracing the probability map of the atlas to the patient's anatomy after the patient has been registered. Later in the second stage, the deformable model was driven by the detection of boundary points along surface profiles. The proposed paradigm was validated using a cross- validation on 36 patients, yielding a reasonable accuracy with a median Dice similarity coefficient of 0.87 [77].

Thereafter, in 2011 Dowling et al. presented a swift fully automatic paradigm which encompassed a dynamic multi-atlas label fusion technique for segmenting the prostate from 3D MRI. A contrasting result was provided when an average shape atlas and the multi-atlas approach were evaluated using the same clinical dataset and manual contours from 50 clinical scans. The proposed method generated a median dice similarity coefficient of 0.86 with an average surface error of 2.00 mm. For non-rigid registration the diffeomorphic demon's method was employed and a comparison of alternate metrics for atlas selection was presented [30]. Also, Gao et al. in 2011 presented a coupled framework including the atlas-based methods and active contours. The proposed paradigm was evaluated on 2 different datasets one of which had 30 images of 15 patients downloaded from publicly available repository and the other included 9 sets of MRI collected from the brigham and women's hospital. This method effectively yielded mean DSC of 0.79 and 0.81 for the respective datasets. The method aimed at using the two widely used families of techniques in order to exploit each's advantage [35]. Mohammad et al. suggested an auto contouring approach utilizing region growing with initial seed followed by canny edge detector for prostate segmentation. This approach overcomes the uncertainties caused due to positioning errors by different registration algorithms [78]. Also Subudhi et al. in 2016 used region growing for segmentation of prostate from MRI. The algorithm starts with dividing the image into blocks having non-overlapping regions. Image was then fourier transformed with output block same as input block. The seed point for region growing was selected by using threshold operator [103].

4.2.3 Thresholding based segmentation approaches

Thresholding is an approach of partitioning the image into foreground and background in such a way that foreground contains the desired region of interest and background is everything else foreground. The working principle of the approach is selecting a threshold value for assigning labels below and above thresholds, to get the segmented image [42]. Some of the approaches used by researchers for segmentation of prostate using thresholding are as follows:

Ozer et al. in 2010 utilized thresholding to perform segmentation of the prostate using a support vector machine and relevance vector machine. Support vector used hyperplane in higher dimensional feature space based on the maximum margin. Whereas, a relative vector uses a probabilistic method with the same function as that of a support vector. Further, the threshold was used to select equal distances, assuming test data equally likely from two classes [82]. Thereafter, in 2012 Gopinath suggested segmentation of prostate from MRI using thresholding based segmentation followed by watershed and morphology. Also, delineation of cancerous region was performed to identify it as malignant or benign [44].

4.2.4 Clustering based segmentation approaches

Clustering is an iterative approach of grouping a cluster in such a way that the objects having similar behavior lie on one group, while rest on another group based on similarities. It is based on the value of distance function, density function, a number of clusters and thresholds to be formed [33]. Some of the approaches used by researchers for segmentation of prostate using clustering are as follows:

Guo et al. in 2014 presented an automated approach for segmentation of prostate using fuzzy c means clustering. This method was based on a combination of multiparametric MRI, which obtains fuzzy information of cancerous tissue. Thereafter, a fuzzy fusion operator on the basis of the Bayesian model and gibbs penalty was applied, which produces maps of

membership degree for the desired region of interest [46]. Rundo et al. in 2017 also suggested clustering based unsupervised machine learning approach for segmentation of prostate from multiparametric MRI. The value of dice similarity coefficient in this case of multiparametric was 90.77 ± 1.75 which was better than processing mono parametric individually [94].

4.2.5 Deep learning-based approaches

Deep learning is a class of machine learning with multiple layers to extract high level functions where lower layers can be used to identify edges and higher layers can be used to identify meaningful information [61]. Commonly used deep learning approaches for prostate cancer are as follows:

Clark et al. in 2017 presented a fully automatic algorithm for delineation of the prostate gland and transition zone (TZ) in diffusion-weighted imaging (DWI) via a stack of fully convolutional neural networks. Two ConvNets were included in a successive manner to perform the segmentation task. The proposed paradigm was assessed by applying it to DWI of 104 patients and produced the median dice similarity coefficients of 0.93 and 0.88 for the prostate gland and TZ respectively. The algorithm eliminated the necessity for the radiologist's intervention in locating the prostate containing slices by automatically detecting the slices containing the portion of prostate gland and then segmenting with an average accuracy of 0.97 [26]. Further, Karimi et al. in 2018 gave a CNN-based method for prostate segmentation in MRI that employed statistical shape models. Very large number of parameters posed a major challenge for the proposed model. The proposed paradigm synthesized additional informative training data by exploiting the knowledge about the expected shape variations and the effectiveness of the regularization techniques that could augment the performance of the trained model. A stage wise training strategy was employed including the data augmentation methods whereby the prostate surface key points were deformed in accordance with the displacements computed based on the shape model. The training dataset consisted of 49 T2-weighted axial MR images. The method achieved a Dice score of 0.88, which was obtained using both elastic net and spectral dropout for regularization [58]. Later in 2018 To et al. proposed a 3D deep dense multipath CNN for the prostate segmentation in MRI. The proposed architecture employed two independent datasets to assess its performance. The network was successively composed of an encoder and a decoder processing block. Also, among the three variants of the proposed network, 3D DM-net-4 feat demanded the longest training time whereas 3D DM-net-16 feat entailed the shortest training time. The first dataset consisted of 100 training cases and 50 testing cases which achieved the DSC of 95.11 with less than 0.80 standard deviation. The results confirmed the robustness to the intrinsic alterations in signal intensities and shape of the gland in the proposed network. Employing the second dataset comprising 30 testing cases yielded dice coefficient on an average of 89.01 [108]. Also, Hossain et al. in 2018 developed a novel model to automatically segment the MRI images of the prostate region using a VGG19-based fully convolutional neural network. The proposed algorithm worked on identifying a region of interest in the image using semantic segmentation, a pixel-wise classification of the content of the input image. Adding residual/skip connections between neighboring and distant layers created a semantic segmentation structure thereby demonstrating the contribution of residual connections in FCN to obtain a greater accuracy in semantic segmentation. The proposed deep learning method achieved a mean intersection-over-union (IU) accuracy of 91.48% and a dice similarity coefficient (DSC) of 94.57% [51]. After that with few modifications, Zhu et al. developed a fully automatic approach to segment

the prostate outer contour and the peripheral zone (PZ) contour with high efficacy. The cropping of the region of interest on DWIs and cascading of two fully convolutional networks on T_2WIs ameliorated the performance especially for PZ identification. The DSC was used as the objective function thus averting the learning process to get trapped in local minima and as a result not being able to obtain a convergence model. To efficiently assess the proposed algorithm, 1416 prostate MR images from 163 subjects were collated. The mean DSC achieved for the proposed method was 92.7 ± 4.2% for the WG and 79.3 ± 10.4% for the PZ [121]. Similarly, Tian et al. in 2018 developed a fully convolutional neural network (CNN) to automatically pixel wise segment the prostate on T2-weighted (T2W) MRI. The algorithm was applied on three data sets containing prostate MRI of 140 patients. Using FCN for image segmentation provided the advantage to use the entire image as an input to the network for both training and testing stages. It led to an efficient prostate MRI segmentation in about 4 s. Caffe was used for implementation of the proposed method. In contrast to the manual labeled ground truth, the proposed CNN model of prostate segmentation (PSNet) obtained a mean dice similarity coefficient of 85.0 ± 3.8%, RVD of 4.1%, HD of 9.3 mm and ASD of 3.0 mm [107]. Recently, Hassanzadeh et al. in 2019 developed and analyzed eight disparate FCNNs based deep 2D network paradigms for automatic MRI prostate segmentation. Large number of segmentation results had a mean DSC between 0.8 and 1.0 when evaluated on the PROMISE12 dataset with ten-fold cross-validation. The presented analysis resulted in a non-bypass dense model unsurpassed by all eight proposed networks for prostate segmentation. To further improve the performance of segmentation, the proposed method incorporated the analysis of various structures of shortcut connections together with the size of a deep network considering MRI slices, MRI volumes and test folds. The non-bypass dense model outperformed all other models with 0.873 mean DSC [49].

4.2.6 Hybrid based approaches

Hybrid approach is a combination of two or more approaches in a defined order to extract the desired region of interest [54]. Different hybrid approaches used till date for segmentation of prostate are as follows:

Liu et al. in 2009 proposed a novel unsupervised segmentation algorithm for prostate cancer. The fuzzy markov random fields (fuzzy MRFs) were employed for the segmentation of prostate from MRI. The algorithm is based on allowing each pixel to belong simultaneously to more than one class. The presented algorithm incorporated a novel strategy of clustering the data and estimating the parameters defining the markovian distribution of the measured data simultaneously. The proposed method when compared with the K-means for MRF parameter estimation and segmentation yielded an improved specificity, sensitivity and accuracy of 99.85%, 99.37%, 99.76% respectively [70]. After a few years in 2015, Alvarez et al. presented an automatic prostate segmentation incorporating a novel SURF based similarity metric and additionally employed a label fusion process. The model was evaluated using a public dataset PROMISE12, composed of 50 MRI cases and comprising 24 MRI acquired with an endorectal coil. Taking the vantage of both the individual shape variation and intra individual salient point representation, the proposed algorithm retrieved similar prostate MRI from the dataset, which were then non-rigidly registered towards a new MRI. The method achieved a robust shape representation from a reduced space of atlases. The proposed method achieved the DSC of 0.79 ± 0.10 with 10 numbers of atlases [8]. Further, in 2016 Tian et al. used superpixels as the elemental processing units and developed a 3D superpixel-based graph cut algorithm to obtain

the prostate surface. The presented method yielded a mean dice ratio of 89.3% on 43 MR volumes. The proposed algorithm used a hybrid 3D method that employed a combination of graph cut and active contour model in a recursive manner to segment prostate MR images. Additionally, for reducing the computational and memory costs, the proposed solution made the shape and gray features robust, which further reduced the prospect of labeling the superpixels with wrong labels. The dependence of the presented semi-automatic method on the initial over segmentation called superpixel acted as a limitation of the proposed algorithm [106]. Thus, Chilali et al. in 2016 gave an automatic paradigm to segment the prostate and sequester the peripheral and transition zones. The proposed algorithm used a two-stage process. Before the employment of the evidential c-means clustering for segmentation, the target image was registered with each zonal atlas image. The approach proved to be ineffective for prostate segmentation extremities, base and the apex, nevertheless the results were in close proximity of the expert contours in the central part of the gland. Based on the experimental evaluations on a representative and multi-centric image, the algorithm yielded a mean DSC of 0.81, 0.70 and 0.62 for the prostate, transition and peripheral zones respectively [24]. Further, in 2017 Reda et al. used an emerging geometric deformable model to segment the DW-MRI images. The model employed the nonnegative matrix factorization (NMF) and extracted discerning features by fusing image intensities in the nearest 10-neighborhood of every voxel, appended with voxel-wise prior and background probabilities of the prostate region. After segmenting the prostate by clustering the voxels of the test image in the H-space, the final segmentation was performed by the deformable model. The proposed method managed in getting the overall DSC of 0.86 ± 0.04, absolute relative volume difference (ARVD) of $1.6 \pm 3.2\%$, and Hausdorff distance (HD) of 5.8 ± 2.1 mm reflecting the high levels of accuracy for the developed segmentation compared to other models taken into consideration [88].

Finally, Table 4 presents the summary of all the segmentation approaches used by different researchers from time to time as discussed above and Table 5 presents the comparison of broadly used state of the art segmentation approaches with pros and cons of each approach.

4.3 Classification

The section presents the classification approaches used by different researchers till date across the globe. The approaches used are categorized into machine learning, deep learning and hybrid. Machine learning classification techniques involve Support Vector Machines (SVM), random forest, k-nearest neighbor (kNN), gradient boosting, logistic regression, naive bayes etc. The deep learning approach comprises deep neural networks and convolutional neural networks etc. Finally, the hybrid category includes a combination of machine learning and deep learning techniques for classification.

4.3.1 Machine learning based approaches

Parfait et al. in 2012 reported an automated classification technique for prostate cancer spectra using magnetic resonance spectroscopy (MRS). The set of features were extracted using spectra i.e. phase and baseline correction, normalization and estimation of metabolites concentration. The study involved the use of SVM and NN classifiers. The results showed that nuclear magnetic resonance spectra are sensitive enough to categorize healthy and cancerous tissues using SVM. Thus, the best results were obtained using preprocessed spectra without quantification taken as input for classification. But the approach can be further improved by

Table 4 Summary of Segmentation Approaches

Author	Year	Approach	Dataset	Performance Measure	Pros	Cons
Samiee et al. [96]	2006	Semi-automatic algorithm	2 MRI volumes with 19 slices each	DSC: 0.8856 using deflated endorectal coil and 0.9057 using inflated endorectal coil	Time efficient	Does not incorporate flexible and modifiable boundary.
Zhu et al. [118]	2007	Hybrid method including 2D and 3D ASM	26 MRI with 288 slices	Root mean square distance Mean: 5.4811 SD: 2.9082	Consistent with capturing the 3D surface of the target object	Manual annotation used to construct the training shapes
Flores-Tapia et al. [32]	2008	Semi-automatic segmentation Based on wavelet multi scale products	MRI volume formed by 19 slices	Mean DSC index: 0.93±.005.	More effective in determining the boundary and discriminating noise at the same time	Does not show the practical feasibility on 3D volumes
Liu et al. [70]	2009	Unsupervised segmentation method based on gaussian model and MRF model	MRI dataset of 11 patients	Specificity, sensitivity and accuracy of 99.85%, 99.37%, 99.76% respectively and DSC: 0.9889	No need to explicitly estimate the parameters	Non-robust to distortions and blurring
Martin et al. [77]	2010	Automated segmentation model using probabilistic atlas	MRI of 36 patients	DSC: 0.87	Fully automatic	Occurrence of error due to single atlas
Gao et al. [34]	2010	Unified shape-based framework	33 MRI prostate data sets	DSC: 0.84 and 0.95, HD: 8.10 mm	Time efficient	User provided input needed to locate the center
Ozer et al. [82]	2010	Thresholding	MRI of 20 patients	AUC with significant difference of 0.12	Improved area under curve	The approach doesn't work well for low contrast images.
Dowling et al. [30]	2011	Multi-atlas segmentation technique	50 clinical scans	Median DSC - 0.86	Improved accuracy with average surface error	Incompetence in identifying accurate segmentation
Gao et al. [35]	2011	Atlas based method and active contours	Dataset 1-MRI of 30 data sets from 15 patients, Dataset 2–9 sets of MRI data from the Brigham and Women's Hospital	Mean DSC of 0.79 for dataset1, mean DSC of 0.81 for dataset2	Improved segmentation	Requires user initiation

Table 4 (continued)

Author	Year	Approach	Dataset	Performance Measure	Pros	Cons
Liu et al. [21]	2011	Shape-based active contour model with level set framework	DWI MRI of 10 patients	DSC of 0.810±0.050, MAD of 2.67± 0.650 mm and HD of 9.07± 1.64 mm	Generic approach	Requires more testing
Malmberg et al. [75]	2012	Smart paint	PROMISE 12	DSC (first round): 0.82 (Second round): 0.86	Generic approach	Not automated
Chandra et al. [22]	2012	Patient specific prostate segmentation	50 clinical MR scans	Mean DSC: 0.85	Case specific	Non-robust
Gopinath [44]	2012	Thresholding	–	–	Robust approach	Requires user involvement for initiation
Guo et al. [46]	2014	Segmentation via distributed discriminative dictionary and ensemble learning	Dataset 1- internal dataset Dataset 2- MICCAI 2012	DSC (first data set): 0.891, DSC (second data set): 0.874	High level of accuracy	More computation
Guo et al. [46]	2014	Fuzzy c means clustering	MRI of 8 patients	DSC: 0.97±0.01	Improved location	Less number of images are used for validation
Alvarez et al. [8]	2015	Novel SURF-based similarity metric	PROMISE12, composed of 50 MRI cases	DSC: 0.79±0.10 with 10 number of atlases	Robust approach	Complex in nature
Tian et al. [105]	2015	Graph cut algorithm	12 prostate volumes	DSC: 0.869 HD:7.2 mm	Easy computation	Use large memory
Tian et al. [106]	2016	3D superpixel-based graph cut algorithm using active contour model	43 MR volumes	Mean dice ratio of 89.3%	Robust and efficient	Dependence on semi-automatic superpixel method
Chilali et al. [24]	2016	Gland and zonal segmentation using c-means clustering	Data set 1- PROMISE 2012 Data set 2–22 patients from five sites	Mean Dice accuracy values of 0.81, 0.70, and 0.62 for the prostate, the transition zone, and peripheral zone	Fully automatic	Validation using only single expert
Subudhi et al. [103]	2016	Region growing	Clinical dataset	Accuracy: 0.68, Sensitivity: 0.54, Specificity: 0.69	Robust in nature	Less accurate
He et al. [50]	2017	Active shape model, adaptive feature learning probability	MICCAI PROMISE12	Mean Dice score of 84% with a standard deviation of 4%	Robust and fully automatic	Less accurate

Table 4 (continued)

Author	Year	Approach	Dataset	Performance Measure	Pros	Cons
		boosting tree and CNN deep learning				
Guo et al. [47]	2017	Unified the deep feature learning with the sparse patch matching	66 T2-W MRI	DSC:87.8±4.0 Precision:91.6±6 Hausdorff:7.43±2.82 mm ASD:1.59±0.51	Effective and robust	Requires testing on large dataset.
Clark et al. [26]	2017	CNN	DWI images of 104	Median DSC of 0.93 and 0.88 for the prostate gland and TZ with average accuracy of 0.97	No need for user intervention to find the prostate gland	Accuracy not upto the mark
Reda et al. [70]	2017	Geometric deformable model	53 clinical DW-MRI data sets	DSC of 0.86±0.04, absolute relative volume difference of 1.6±3.2%, and HD of 5.8±2.1 mm	Non-invasive approach of detection	Less automated
Rundo et al. [94]	2017	Fuzzy c means	Clinical dataset comprising of 21 patients	DSC of 90.77±1.75	Robust in nature	Time consuming
Karimi et al. [58]	2018	CNN-based method using statistical shape models	49 T2-weighted axial MR images	Dice score of 0.88	Improved performance	Needs large number of parameters
To et al. [82]	2018	Multi-path CNN	Data set 1–100 training cases and 50 testing cases Data set 2–30 testing cases	Data set 1 – 95.11 DSC and < 0.80 SD Data set 2 – DSC of 89.01 on average	Robust and accurate	Time consuming
Zhu et al. [108]	2018	Cascaded U-Net	1416 prostate MR images from 163 subjects	DSC - 92.7±4.2% for the WG and 79.3 ±10.4% for the PZ	Fully automatic	Time consuming
Tian et al. [107]	2018	Deep full CNN	Prostate MRI of 140 patients	DSC:85.0±3.8% RVD: 4.1% HD:9.3 mm ASD:3.0 mm	Entire image to be used as input in training and testing phases	Accuracy is not upto the mark
Hassanzadeh et al. [49]	2019	Analyzing 8 deep FCNN based 2D network structures	PROMISE12 dataset with ten-fold cross--validation	Non-bypass dense model with mean DSC of 0.873	Improved performance	Requires testing on diverse datasets

Table 5 Comparison of Denoising approaches

S.No.	Approach Used	Pros	Cons
1	Contour and Shape based [66]	It is a robust, versatile and efficient approach. Handle sharp corners with topological changes.	Construction of efficient velocity for the level set function is time-consuming. Under and over-segmentation.
2	Region/Atlas based [91]	Provide better segmentation performance.	Requires initial seed, making it less automated. High time complexity.
3	Thresholding [42]	Does not require prior information of the image.	It does not work well for images with a broad and flat range of pixels.
4	Clustering [33]	Reduce false blobs. Obtain homogeneous and heterogeneous regions.	Sensitive to initialization for a number of clusters and center
5	Deep learning [61]	Automated in nature	High time and space complexity.
6	Hybrid [54]	It includes the desirable properties and excludes the undesirable properties of each of the approaches in hybrid segmentation.	High time and space complexity.

automating the system for better results. Further, the undetermined spectra could be classified for improved performance [83]. In the same year, Shah V et al. presented a decision support system for localizing PCa using mp-MRI. The study confined to peripheral Zone PCa and identification of cancer and normal regions in PZ by correlating with previous histology specimens. Segmented regions on mp-MRI were projected on histopathology and were used as a training set for decision support system (DSS). Thereafter, the machine learning approach was performed on the training set and cancer probability maps were obtained. Finally, the additional evolutionary i.e. genetic algorithmic approach was implemented to get the optimal values of parameters. Also, the cross validation was placed with non-optimized SVM and optimized SVM. Thus, the authors projected that the system should follow up an active surveillance system in future for better diagnosis [99]. Later in 2014, Lehaire et al. gave the CAD system for detection of PCa combining sparse dictionary learning and supervised classification methods. The study is confined to voxel-based detection in peripheral zones using mp-MRI. Feature extraction was performed in collaboration with supervised classification and learned dictionaries. Thus, the classification methods were used to determine the normal(N), normal but suspect (NS) and other classes of cancer. The level of cancer was decided on the basis of gleason score ranged from 6 to 9 and the classification was performed using supervised classifiers namely support vector machine (SVM) and logistic Regression. But the use of sparse dictionary learning techniques was not able to improve the performance. Thus, perspective deep learning methods can be associated with nonlinear supervised classification for obtaining cancer probability maps in correlation with gleason score [1]. Also, Lemaitre et al. in 2015 proposed a unique approach for prostate cancer detection using mp-MRI. But with the passage of time, diagnosis has become more serene for the patients and experts as many of the parameters reduce its efficacy and increases the chances of detecting the potential lesions at an early stage. Thus, various computer aided detection and diagnosis techniques are developed and implemented. This study introduced a boosting approach in the form of classifier i.e. gradient boosting classifier. Initially the automated detection of PCa was done in per voxel manner with 3 T mp-MRI and the classification was performed using 3D text tone based strategy. Authors suggested that registration and segmentation of mp-MRI data should be discarded and applied before classification and features other than intensities for

improved performance [62]. Similarly, Fehr et al. in 2015 proposed automatic classification of prostate cancer on the basis of gleason scoring system. The study introduced the project of machine learning based classification in collaboration with apparent diffusion coefficient (ADC) and T2 weighted MRI extracted features. The results showed that classification on the basis of gleason scores was more accurate despite the involvement of highly imbalanced data. The study was confined only for peripheral and transition zones with the validation of the results by Pz and Pz, Tz in combination. The available data on Tz alone was not sufficient as per the study and was found to be a major setback of the research. Thus, the results were based on a retrospective dataset with no true validation. Authors also suggested that voxel wise classification could be used to further improve the results [65]. Further. Trigui et al. in 2017 presented a tool for automatic classification and localization of prostate cancer using MRI and Magnetic Resonance spectroscopy Imaging (MRSI). As the efficacy of detection and localization of cancer prone tissues increased with the proposed classifiers. The study described the implementation of SVM and random forest-based classification techniques. It categorized the segmented regions into three classes (Healthy, Benign, Malignant). The use of MRSI was introduced in the study with MRI to compare with Parfait et al. [83] and was found to improve the performance of classification along with quality of spectra as accuracy of global detection of the extracted features enhanced by Mp-MRI. SVM classifiers were also tested for healthy and malignant voxels and the random forest classifier for all the classes were included with benign cases. The results were mapped on the color-coded maps (CAD tool). Global detection was thus improved by modifying automatic classification and 3 D voxel neighborhood and the size of the dataset made the results more robust. Further, analyzing and filtering 3D shape tumours enhanced the efficacy [31]. In the same year, Liu et al. presented the CAD system using multimodal MRI and targeted biopsy labels. The new PCa classification method was introduced in the study which involved the integration of T2 weighted, diffusion weighted and dynamic enhanced MRI images. Images were initially encoded in the DICOM format and the system consisted of three steps. First the registration of modalities took place and then in the second step, features were extracted to capture intensity and texture information of targeted labels. Lastly, SVM and supervised learning methods were performed to detect suspicious cancerous tissues. Further, the large dataset could be used to make the system more robust and improve the results. Also, integration of other modalities could be implemented for the same [109]. Recently, in 2018 Li et al. performed classification of prostate cancer on the basis of gleason score using SVM. This study involved mp-MRI segmented images as input. After segmentation gleason score was assigned to the level of prostate cancer. The study confined only to central gland (CG) and on the basis of extracted features with mp-MRI eleven parameters were deprived through histogram analysis including mean, median, 10th percentile, skewness and kurtosis. The model was thus developed with 10-fold cross validation and the end results were checked with two separate datasets. The results showed better accuracy for classification with gleason score of PCa. Further, the authors suggested that validation and analysis of the outcomes could be cross checked with more datasets to support the diagnostic value of automated method [71]. Thus, solving the problem of accuracy and classification imbalance, Abraham et al. in 2018 presented the collaboration of sparse autoencoder and random forest classifier instead of softmax classifier. Three additional techniques were developed in this study. Synthetic minority oversampling technique (SMOTE), weka resample algorithm and adaptive synthetic (ADASYN) sampling were the approaches introduced in the study. High level features were extracted in the same way as single layer sparse autoencoders. Further, the grade was investigated with the use of mp-MRI biomarkers and the highly

imbalanced dataset was taken in the ADASYN. The performance metrics were validated with many classifiers but random forest achieved better results in comparison with others. Accuracy and f-score increased up to a great level unlike in the previous study. Also, the automation of the complete system could produce much better outcomes and reduce the manual approaches [67]. Similarly, Reda et al. in 2018 developed a CAD system for early diagnosis of PCa. They used clinical biomarkers based on prostate specific antigen (PSA) integrated with extracted features from DW-MRI at different b values. The framework used constituted three steps, i.e. prostate delineation, estimation and normalization of diffusion parameters and integration of PSA based probabilities with initial probabilities acquired using stacked non-negativity constraint sparse autoencoders. Autoencoders involved the use of ADC cumulative distribution functions for better accuracy. Transformation of PSA resulted in diagnostic probabilities was done by a kNN classifier. Further the number of participants can be enhanced for robustness and different cases of b values can be used for better accuracy [2]. Also, with few modifications Xu et al. in 2018 also reported an automated classification method for categorizing of PCa using gleason scores. This work involved the automatic gleason grading of PCa using H&E stained (digitized) whole slide biopsy images. The grading mechanism used completed and statistical local binary patterns (CSLBP) descriptors. The whole slide images initially separated out salient tumour tiles with high nuclei densities. Thereafter, the CSLBP textural features were extracted to categorize gleason patterns into normal and abnormal cases. At the end, CSLBP features were computed, augmented and utilized by multi-class SVMs with assigned gleason scores to the biopsy. The SVM classifications results were then tested against polynomial and gaussian kernels. Finally, the results showed that Gleason grading with CSLBP was more accurate than state of the art textural features and the use of CSLBP in other types of cancers could be of great significance [89].

4.3.2 Deep learning-based approaches

Liu et al. in 2017 projected a classification framework for PCa based on deep learning. This study presented the imaging diagnosis method to ease the MRI dependence on expert skills and experiences. The framework comprises convolutional neural networks (CNN) which is an image classification model. The data used for experimentation was divided into two subsets i.e. training and testing. The framework is confined with prostate cancer in the study but can be used for other tasks of cancer as well. Grading and staging of PCa can also be left alone as an area in this research [69]. Also, Abraham et al. in 2018 described the idea to classify the prostate cancer grade groups using advanced extracted features. Initially, the high-level features were extracted from handcrafted texture features including the implementation of DNN stacked sparse autoencoders (SSAE). After feature extraction classification of PCa grade were analyzed using mp-MRI biomarkers, placed with newly introduced softmax classifier (SMC). The results were found to be quite better on the dataset containing 112 training and 70 testing images. Positive predictive values (PPV) and kappa score were the parameters discussed in outcomes. The approach could be reduced with better mp-MRI modalities and techniques [3]. Similarly, Ishioka et al. in 2018 presented a fully automated CAD algorithm for the detection of PCa based on MRI. The study focused on global standardization and variability problems. Introduction of CAD algorithm with convolution neural network (CNN) reduced the extent of problems encountered in the state of the art. CNN was then validated on training and testing data to achieve improved results. Thus, for comparison graphics processing unit (GPU) algorithms were implemented and different receiver operating

curves were analyzed. Automation of deep learning provided reproducible interpretation and thus the algorithm could be tested against more datasets to check robustness of algorithms in future [56]. Recently, Yuan Y et al. in 2019 presented an automated classification system for PCa using mpMRI transfer learning model. PCa classification was performed on the gleason scoring system and the study gave accurate and risk-free results. The study projected multiparametric magnetic resonance transfer learning (MPTL) method to automatically classify PCa. Firstly, three stages CNN were developed to determine features from mp-MRI (T2w, ADC). Thereafter, the extracted features were correlated to represent information of mp-MRI sequences and the additional image similarity constraints were involved to distribute the features in narrow angle regions. Based on the analysis, authors suggested that with point constraints of softmax loss and image similarity loss in tuning process could provide features with intraclass compactness and interclass separability [117]. Also, UCLA technology development group in 2019 developed deep learning based computerized classification technique using a hierarchical framework. The classification system was strictly based on mp-MRI images. The development group invented an automated algorithm for analysis of mp-MRI images using a deep learning approach. The algorithm was not confined to PCa only, as it could be used for other areas as well. The biggest advantage of this technique was that it did not require precise lesion boundaries for accurate analysis and is not only restricted to a smaller number of training samples, solving the problem of robustness [111].

4.3.3 Hybrid based approaches

Niaf et al. in 2012 presented a CAD system with a feature set acquired from gray-level images. The image features such as first order statistics, haralick features, gradient features, semi-quantitative and quantitative (pharmacokinetic modeling) dynamic parameters were initially extracted. The approach is confined only to the peripheral zone for the determination of PCa based on mp-MRI. Based on the study, use of four sets of classifiers i.e. nonlinear support vector machines (SVM), linear discriminant analysis, nearest neighbors and naive bayes were analyzed. The classifiers were trained using supervised learning on the basis of t-test mutual information, minimum redundancy and maximum relevance criteria to compare with a set of feature selection techniques. Authors also revealed that the in-depth study of evaluation of the radiologist's performance with and without CAD systems could be of great significance [81]. Later, Wang et al. in 2017 reported fully automated MRI classification based on pathologically confirmed PCa patients. The study involved the use of deep learning and non-deep learning for classification and comparison of the outcomes with existing state of the art. Deep learning constitutes of convolutional neural network (CNN) also termed as DCNN, while non-deep learning methods with image recognition and analysis was performed using SIFT image feature and bag-of-wood (BoW) with SVM. Thus experimental results showed that DCNN gives considerably higher AUC than non-deep learning. Also, the authors revealed that fully automated systems are of more significance than semi-automated systems. This study further reduced the manual computation and increased the automation for lesions segmentation. But, more effective DNN can be developed with least dependency on the patients. Another future perspective could be checking the robustness of a system with additional quantitative features [113]. Also, Yang et al. in 2017 projected a co-trained convolutional neural network for diagnosis of prostate cancer. A weakly supervised CNN used in the study for localization of PCa lesions used mp-MRI. The augmented method guided CNN to observe true features and dominate the irrelevant patterns. This work was based on deep CNN and one stage SVM

classifier to concurrently categorize the presence of lesions in the MRI image. Further, the additional back propagated error E was introduced for optimized classification results and consistent cancer response maps. Using these maps highly representative PCa relevant features were acquired which led to more accurate results. Finally, the analysis revealed that discriminative visual patterns could be learned from lesion locations [115].

Finally, Table 6 presents the summary of all the classification approaches used by different researchers from time to time as discussed above and Table 7 presents the comparison of broadly used state of the art classification approaches with pros and cons of each approach.

5 Performance metrics

These are the values used for analysis of the approaches and is given in section 3.1 for denoising and section 3.2 for segmentation.

5.1 Denoising performance metrics

5.1.1 PSNR

PSNR is the ratio between corrupted noise power that affects the visual representation of an image and maximum possible power of the signal. This is represented in terms of logarithmic scale due to dynamic range of signals [53]. PSNR is defined as

$$PSNR = 10.\log_{10}\left(\frac{{MAX_i}^2}{MSE}\right) \tag{1}$$

Here, MAX_i is the maximum value of the pixel within the image and MSE is mean square error.

5.1.2 MSE

It is the measure of average errors of the squares calculated as the difference between what is estimated and the estimator. This corresponds to the expected value of loss in square as a result of difference due to randomness [63]. The MSE is given as

$$MSE = \frac{1}{m \times n}\sum_{i=0}^{m-1}\sum_{j=0}^{n-1}\left[I(x,y) - I'\left(x,y\right)\right]^2 \tag{2}$$

Here, $m \times n$ are the dimensions of image, is the initial image and $I'(x,y)$ is image after estimation. The value of MSE is always positive and the one with less value is considered good.

5.1.3 SSIM

SSIM is the measure of similarity within two images which describes quality based on the initial manipulated image as reference. It considers degradation in image as change perceived in structural information, including both contrast and luminance masking terms. Luminance here is the distortion in the image which tends to be less observable in bright regions, whereas contrast is the distortion which becomes less visible in abrupt changes and textured regions [112]. SSIM is given as

Table 6 Summary of Classification Approaches

Authors	Year	Classifier used	Features extracted	Datasets	Performance measure	Pros	Cons
Parfait et al. [83]	2012	SVM	Voxel based features	22 patient datasets with biopsy proven Cancer	Sensitivity: 83.57%, specificity: 98.11%, error rate: 4.51%	Improved quality of spectroscopy	Classified undetermined spectra
Shah V et al. [99]	2012	SVM	ADC, NT2W, T_1, k^{trans}, k_{ep}	31 patients (mean age and serum prostate specific antigen of 60.4 and 6.62 ng/ml, respectively)	Dss with optimized SVM f-measure:89, Kappa: 80%, Dss without optimized SVM f-measure:85%, Kappa: 75%	Dss produced satisfactory results	Confined to only peripheral zone
Niaf et al. [81]	2012	SVM, linear discriminant analysis, k-nearest neighbours and naive bayes	Gradient, texture, functional, grey level, ROI modeling, image features	30 sets of multiparametric MR images	AUC: 0.89 with SVM (malignant vs nonmalignant) AUC: 0.82 for malignant vs suspicious in combination of t test with SVM	Improved classification results for gray level images	Only works for peripheral zone
Lehaire et al. [1]	2014	SVM and Logistic Regression classifier	Voxel based features	35 patients mp-MRI	LR mean accuracy:0.84 SVM accuracy: 0.72	Improved computational speed	Accuracy not upto the mark.
Lemaitre et al. [62]	2015	Gradient Boosting Classifier	Voxel and 3d texton based features	Dataset with 20 patients comprising of 18 patients with biopsy proven PCa and 2 healthy patients	Sensitivity: 94.7%, specificity: 93%, AUC: 0.968	Improved sensitivity and specificity with reasonable AUC value	Tested on less number of images.
Fehr et al. [65]	2015	Machine learning based classifier	ADC and T2w MRI based texture-based features	T2-W and ADC MR images acquired from 217 men	Accuracy Pz and tz: 92% Pz alone: 93%	Distinguishing gleason scores	Not involved the case solely of transition zone
Trigui et al. [31]	2017	SVM, Random forest	Wash in, texture features, ADC features, enhanced spectra, choline and citrate concentrations	MRI/MRSI data base of 34patients, with 7711 spectroscopy voxels	SVM Sensitivity: 99.1%, specificity: 98.4%, error rate:1%	Improved quality of spectra	High time complexity.

Table 6 (continued)

Authors	Year	Classifier used	Features extracted	Datasets	Performance measure	Pros	Cons
Liu et al. [109]	2017	SVM	Intensity, shape and texture statistical features (biopsy labelled targets)	Dataset of 54 patients that underwent 164 targeted biopsies (58 positive, 106 negative)	SVM with AUC: 0.82 (95% CI [0.71,0.93]), Proposed tri modal algorithm AUC: 0.73(95% CI [0.55,0.84])	Improved space and time complexity	Less number of features were used with chances of missing significant features.
Liu et al. [69]	2017	CNN	–	10,056 diffusion weighted magnetic resonance imaging	Accuracy without training: 64.91%, with training 99.99%	Dependency on experts and their experiences reduced	Grading and staging of cancer were not included
Wang et al. [113]	2017	CNN, DCNN, SVM	SIFT image features	172 patients with 2602 morphologic images	DNN AUC: 0.84 (95% CI 0.78–0.89), non DNN AUC 0.70(95% CI 0.63–0.77)	No manual work for lesion segmentation	Tested for less number of features.
Yang et al. [115]	2017	SVM, CNN	Highly representative PCa relevant CNN features	160 patient data with 12-core systematic TRUS-guided prostate biopsy	For 10 false positives per normal/benign patient sensitivity 0.97	Concurrent lesion detection became effective	Weakly supervised CNN
Li et al. [71]	2018	SVM	10th percentile, mean, skewness, median, kurtosis.,	A2, B2	AUC: 0.99 for A2, 0.91 for B2 with reverse data and AUC 0.99 for B2, 0.90 for A2.	Improved accuracy for gleason classification	Less robust
Abraham et al. [3]	2018	DNN, soft max classifier	High level features	Training set of 112 lesions and a testing set of 70 lesions	Kappa score: 0.2326, ppv: 80.26%	Grading of PCa improvised	Reduced accuracy, Classification of imbalance data
Abraham et al. [67]	2018	Random forest classifier	Features using sparse autoencoder activation function	330 lesions comprising of 76 clinically significant PCa lesions and 254 indolent lesions	Kappa score: 0.873, Accuracy 93.65%, F-measure 0.94, ROC 0.979	No imbalance data classification problem	Automation needed.

Table 6 (continued)

Authors	Year	Classifier used	Features extracted	Datasets	Performance measure	Pros	Cons
Reda et al. [2]	2018	K nearest neighbour	ADC maps and CDFs	Analyses were conducted on DW-MRI data sets acquired from 18 patients (9 benign and 9 malignant)	Specificity 100%, sensitivity 88.9%, accuracy 94.4%	Efficient CAD system for seven cases of b values	Non-robustness
Xu et al. [89]	2018	SVM	CSLBP texture Features	312 different patient cases selected from the cancer genome atlas (TCGA)	Accuracy: 79%	Robust approach	Could not work for other types of cancers.
Ishioka et al. [56]	2018	CNN	–	335 patients with a prostate-specific antigen level of <20 ng/mL	GPU AUC: 0.645 CAD AUC: 0.636	Best diagnostic accuracy	High time complexity.
Yuan Y et al. [117]	2019	Cnn with MPTL	T2w trans axial, T2w sagittal, and apparent diffusion coefficient (ADC)	132 cases from institutional review board-approved patient database and 112 cases from the PROSTATEx-2 Challenge	Accuracy 86.92%	Accurate and risk-free results	Intraclass compactness and interclass separability
UCLA Technology Development Group [111]	2019	Deep learning	Lesion based features	–	–	No need of precise lesion boundaries	Not accurate

Table 7 Comparison of Classification Approaches

S.no.	Approach used	Pros	Cons
1	Machine learning	These approaches have less time and space complexity	Requires extraction of handcrafted features
2	Deep learning	Automated in nature	High time and space complexity
3	Hybrid	Offers improved performance	High time and space complexity

$$SSIM = \frac{(2\mu_F\mu_{F'} + c1)(2\sigma_F\sigma_{F'} + c2)}{(\mu_F{}^2 + \mu_{F'}{}^2 + c1)(\sigma_F{}^2 + \sigma_{F'}{}^2 + c2)} \tag{3}$$

Where μ_F and $\mu_{F'}$ are average of F and F', σ_F and $\sigma_{F'}$ are variance of F and F', $c1$ and $c2$ are variables to stabilize the division using weak denomination, while F and F′ are input images. Here, the higher value of SSIM specifies more similarity and vice versa.

5.2 Segmentation performance metrics [110]

5.2.1 Dice metric

Dice metric is a metric which is used to compare the similarity between two fields i.e. segmented area and ground truth. In this case, it is given as

$$dm = \frac{2 \times Area(A \cap B)}{Area(A) + Area(B)} \tag{4}$$

Here, dm is a dice metric, A is a segmented area and B is an area of ground truth. More is the value of dm better is the performance.

5.2.2 Area overlap

Area overlap is the metric which accesses how well the segmented area matches the actual ground truth area and is given in eq. (5):

$$m1 = \frac{A_{seg} \cap A_{gt}}{A_{seg} \cup A_{gt}} \tag{5}$$

Here m1 is an overlap area ratio, A_{seg} is segmented area and A_{gt} is ground truth area. More is the value of m better is the performance.

5.3 Classification performance metric [120]

5.3.1 Sensitivity

Sensitivity is the probability of diseased occurrence to the total number of diseased occurrences and is given as:

$$\text{Sensitivity} = \text{Tp}/(\text{Tp} + \text{Fn}) \tag{6}$$

Here, Tp is a resultant where the classifier accurately predicts the positive class and Fn is a resultant where the model wrongly predicts the negative class.

5.3.2 Specificity

Specificity is the probability of non-diseased occurrences to the total number of non-diseased occurrences and is given as:

$$\text{Specificity} = \text{Tn}/(\text{Tn} + \text{Fp}) \tag{7}$$

Here, Tn is a resultant where the model accurately predicts the negative class and Fp is a resultant where the model wrongly predicts the positive class.

5.3.3 Accuracy

Accuracy is the state of being precise or correct and is given as:

$$\text{Accuracy}=\text{Tp} + \text{Tn}/(\text{Tp} + \text{Tn} + \text{Fp} + \text{Fn}) \times 100 \tag{8}$$

6 Results and discussions

6.1 Experimental setup

The experimentation was performed in python 3.7 and Tensorflow version 1.13.1 using scikit and skimage libraries for the filters namely anisotropic, bilateral, gaussian, mean, non-local means, median, wavelet and wiener. Furthermore, the execution was performed on the following hardware setup:

- **Workstation:** MSI mobile workstation manufactured by Micro-Star International with model MS-16P6 i.e. MSI WE63 8SI
- **CPU:** Intel Core i7 8th gen 8750H processor
- **Graphics Card:** NVIDIA Quadro P1000 graphics card
- **Frequency:** 1895.4 MHz
- **Bandwidth:** Maximum 1333 MHz

The public dataset discussed in section 1.3 was used for testing of denoising, segmentation and classification approaches. The T2W images from MRI dataset comprising of images in. dcm format was converted into .png for better results. Finally, the performance of denoising approaches implemented were analysed using metrics such as PSNR, MSE and SSIM. Whereas, the performance of shape and contour-based segmentation was analysed using dice metric and area overlap. Further performance of classification was analysed using sensitivity, specificity and accuracy.

Same set of images were used for denoising, segmentation and classification to avoid bias in results. Images were initially corrupted by introducing different types of noises to evaluate the performance of filters. Further, the segmentation and classification were performed on denoised images. The input images used for training and evaluation were initially cropped to 512 X 512 pixels to better train the segmentation and classification models due to increased visibility of ROI especially in case of deep learning architectures. Also, in order to avoid overfitting, data augmentation which is

an approach to increase the number of samples in the dataset was applied. Thus, techniques such as rotation, flipping and zooming were used for data augmentation. First, the images were flipped vertically, which doubled the dataset size. Thereafter, a horizontal flip was given to the images, which further increased the number of images in the dataset.

6.2 Findings

Development of CADs for PCa is one of the challenging tasks that varies with use of different imaging modalities such as CT, MRI, mp-MRI, PET and radiomics. Among all the modalities used, MRI is commonly used as it offers certain advantages over others such as lossless radiations, non-invasive, easy acquisition and less cost. This paper presents the analysis of different denoising, segmentation and classification approaches, which are significant steps for any CADs. Denoising is the phenomenon to remove rician and gaussian noise present in MRI during acquisition using different types of filters. Although different denoising filters have been used by researchers till date for reduction of noise, they suppress the image details and also cause blurring effect due to extra smoothness. While, few others make the computations complex and enhance the cost of treatment as well. Different filters such as non-local means, neutrosophic set wiener filtering, median, anisotropic etc. are used only for certain specific noises. Further, for the computational flexibility, some methods were proposed and implemented in the literature such as chi square unbiased risk estimation, sylvester lyapunov equation and non-local means etc. Though they restricted the complexity of computation yet image details suppression remains a major challenge. In the traditional methods, use of CT images reduced the contrast details of the images which further affected the overall performance of denoising. MRI images solved the problem of lack of details of organs in the other imaging modality. It provided the complete details of the tissues neighboring to cancerous ones. Also, various models like curvelet transform, Gaussian scale mixture etc. were performed to maintain image details. Thus, there is a need for an improved denoising algorithm which reduces the noise without losing the significant visual information from images.

On the other hand, segmentation involves other major challenges such as extraction of over or under region of interests (ROIs), computational complexity and automation. Semi-automatic algorithms were initially appended in traditional manual approaches to reduce the problem of automation. But all these approaches were prone to certain errors such as detection of false ROIs. Thus, patient specific segmentations were performed to enhance accuracy and feasibility but this further increased the time and reduced generalization leading to problems of robustness and automation. Robustness raised an issue in almost all of the segmentation cases and thus a large number of training and testing was suggested. Further, atlas-based methods were implemented to improve the performance. But inflexible boundaries reducing the overall performance of the images were found to be a major challenge to avoid. Also, various hybrid 2D and 3D methods were suggested in literature to get rid of these issues but computational complexity was increased in this case. Thus, a need for a segmentation approach with less computation, automation and improved performance was encountered.

Lastly, the final step of CADs i.e. classification was analyzed. Here, the selection of significant features and classifiers plays a crucial role. Major challenges in the case of traditional classification include extraction of different handcrafted features varying from one study to another. As discussed, classification approaches are divided into three categories i.e. machine learning, deep learning and hybrid. Most of the studies of classification involving machine learning approach faced the problem of desirable accuracy and robustness. Some of the machine learning classifiers like gradient boosting classifier, logistic regression etc. were

introduced to improve the performance of the system. But recently, deep learning has gained a kind attention as it solves the problem of automation but it needs large dataset with a variety of images for training to make the classifier self-learn and perform better in testing. Also, hybrid classification approaches collaborating machine learning and deep learning are encountered to increase reproducibility, automation and robustness but with increased computation. The expansion of involved classification techniques to other cases could lead to a large number of undetermined issues. The studies revealed that the selection of the dataset would decide the overall outcome of the classification. The grading of PCa was improvised with the use of a soft max classifier. But it generated another cumbersome issue of classification of imbalance data. Also, the dataset involved became a great concern. Highly representative PCa relevant CNN features make concurrent lesion detection effective in classification. Most of the involved studies are specific to a few zones only like peripheral zones, transition zones etc.

From the above discussions, challenges involved in denoising, segmentation and classification of PCa were explored. Some of the common perspectives were suppressing of image details and deteriorating the accuracy and robustness. Also, the automation of the approaches made the investigation much better than others.

6.3 Denoising of Gaussian noise

The experimental results for denoising using different filters are given in Figs. 9, 10, 11, 12, 13 and 14 and Table 8.

6.4 Denoising of Rician noise

6.5 Denoising of Gaussian and Rician noise

In case of original image, the one with high error reflects low quality image and hence the lower value of PSNR. Whereas, less error gives better image quality with higher value of PSNR. However other filters such as Wavelet, gaussian, bilateral, anisotropic also give better quality. But anisotropic filter gives an average PSNR of 28.29 and is thus considered the most optimal. Further, in case of gaussian denoised image other filters such as Wavelet, gaussian, bilateral, anisotropic and non-local means also give better quality. But anisotropic filter gives an average PSNR of 28.29 and is thus considered the most optimal. Similarly, in case of rician denoised image, it can be seen that the least value is shown by wiener filter with 27.67 PSNR giving low quality image and highest quality is given by the non-local means filter with 28.25 PSNR. While, other filters such as Wavelet, gaussian, bilateral and anisotropic also give better performance. But the anisotropic gives an average PSNR of 28.06 and is thus the most optimal. Finally, in case of combined gaussian and rician denoised image it can be seen that non-local means gives highest PSNR of 28.61, wiener gives least PSNR of 27.64 and anisotropic gives optimal performance with PSNR of 28.34. Hence the best performance is considered to be of anisotropic filter, as its values lie in median range i.e. neither too high nor too low.

In case of MSE larger values represent the values scattered widely around its mean, and thus the smaller value is preferred as it shows the values are dispersed closely to its mean value. Hence in case of gaussian denoised image the least value is given by the non-local means filter as 95.68 MSE and the other filters such as anisotropic gives MSE of 96.22, bilateral with 97.70 MSE, gaussian with 98.95 MSE, while mean and median give the same value i.e. 101.80 MSE. Similarly, in case of

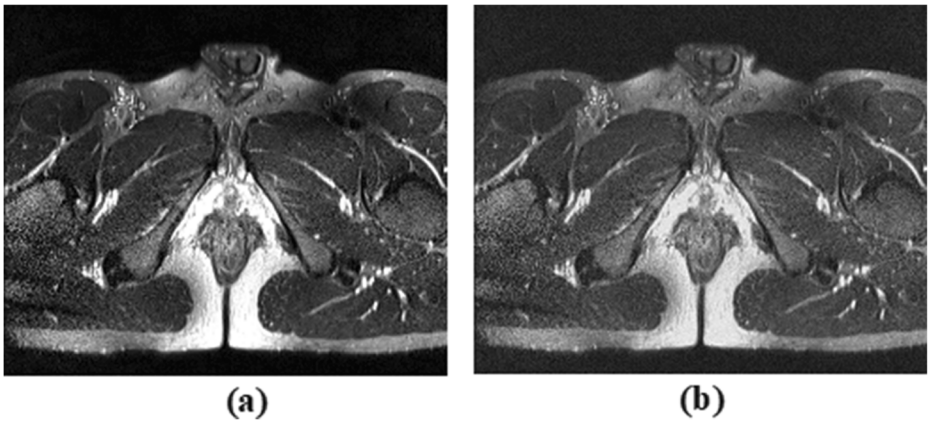

Fig. 9 (a) Original image (b) Image with Gaussian noise

rician denoised image the least value of MSE is observed to be 97.19 for non-local means, and 101.52 for anisotropic, 106.88 for bilateral, 103.75 for gaussian, 102.29 for mean, 105.03 for median, 99.51 for wavelet, and the highest value is given by weiner with 111.10 MSE and so is least

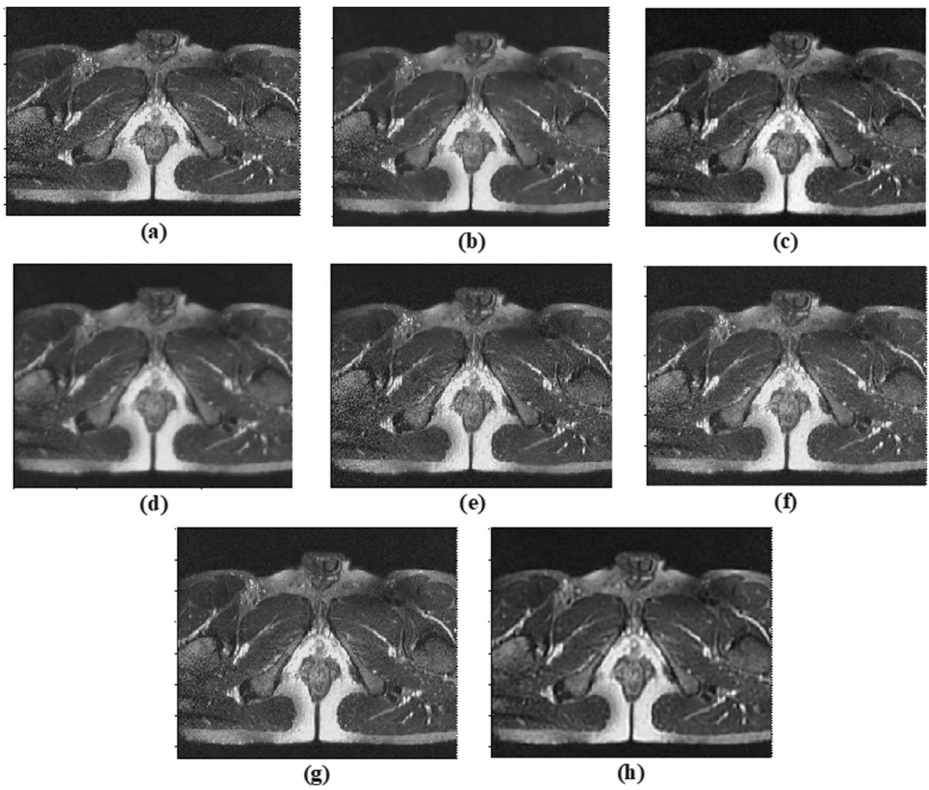

Fig. 10 Filtering of gaussian noise using different filters (**a**) ANISOTROPIC FILTER (**b**) BILATERAL FILTER (**c**) GAUSSIAN FILTER (**d**) MEAN FILTER (**e**) NON-LOCAL MEANS (**f**) MEDIAN FILTER (**g**) WAVELET FILTER (**h**) WIENER FILTER

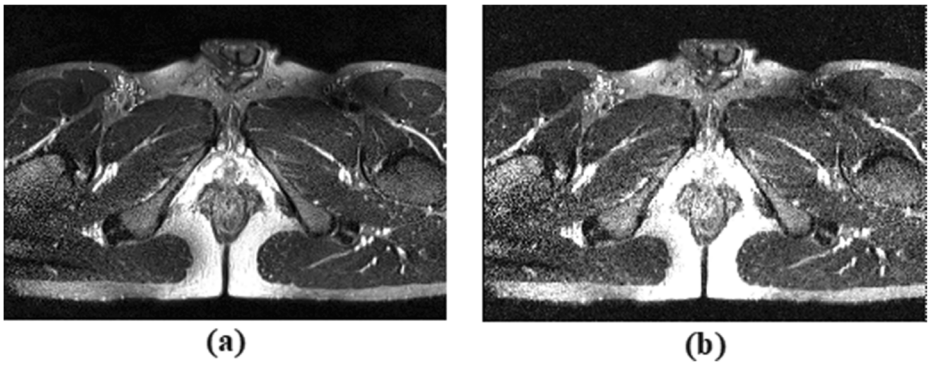

Fig. 11 (**a**) Original image (**b**) Image with rician noise

preferred. Further, in case of combine gaussian and rician denoised image, the least value is given by the non-local means filter as 89.55 MSE and the other filters gives MSE values as 95.13 for anisotropic, 99.74 for bilateral, 97.34 for gaussian, 96.50 for mean, 101.27 for median, 92.89 for

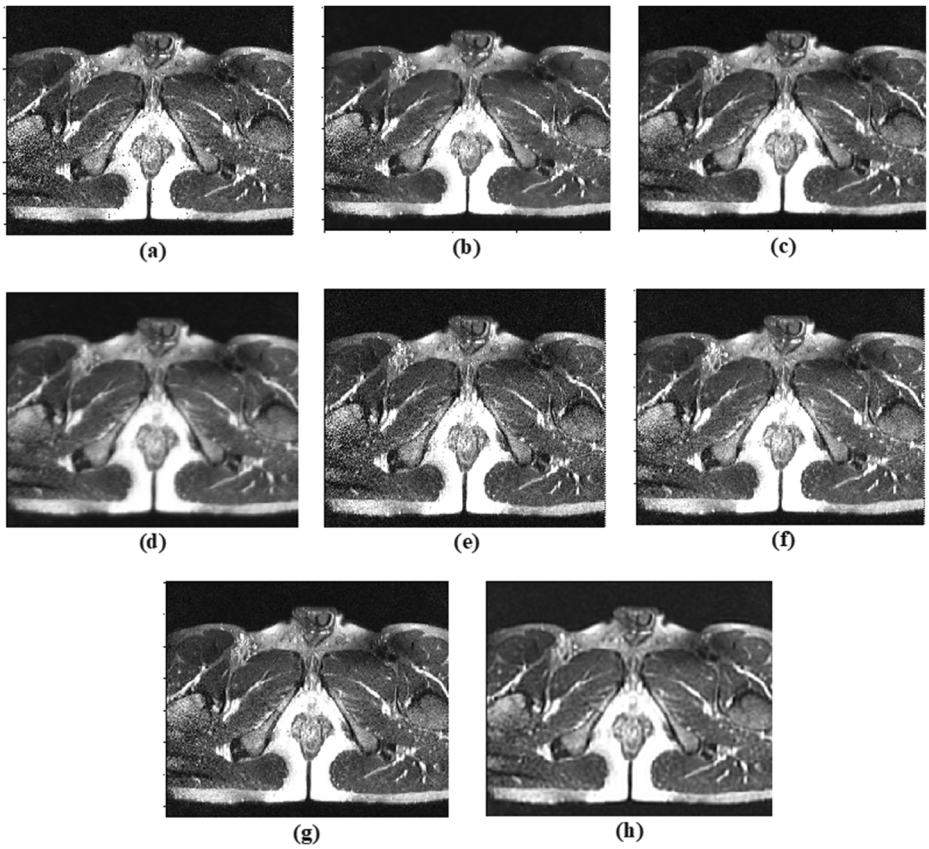

Fig. 12 Filtering of Rician noise using different filter (**a**) ANISOTROPIC FILTER (**b**) BILATERAL FILTER (**c**) GAUSSIAN FILTER (**d**) MEAN FILTER (**e**) NON-LOCAL MEANS (**f**) MEDIAN FILTER (**g**) WAVELET FILTER (**h**) WIENER FILTER

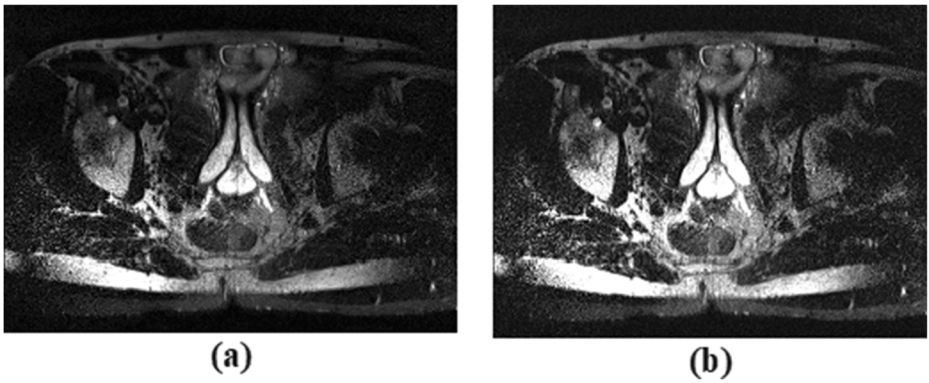

Fig. 13 (**a**) Original image (**b**) Image with gaussian and rician noise

wavelet, and the highest value is given as 111.92 for wiener and so is least preferred. But anisotropic performs optimally with an average MSE of 96.22 for denoised gaussian noise image, MSE of 101.52 for denoised rician noise image and MSE of 95.13 for denoised gaussian and rician noise

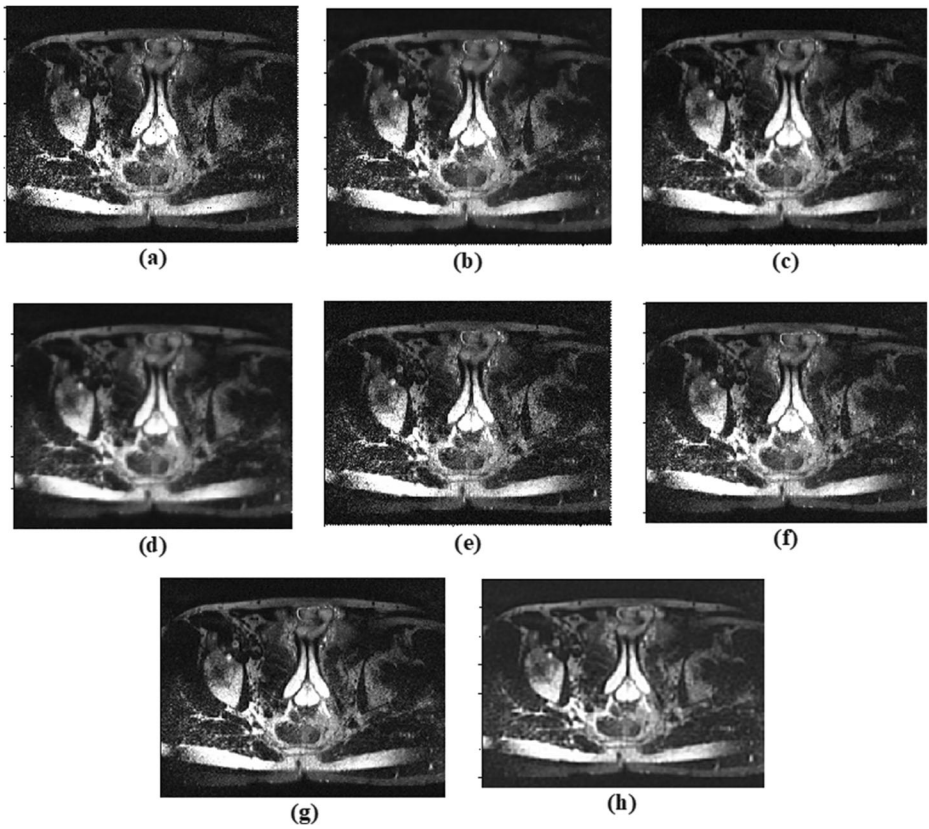

Fig. 14 Filtering of Gaussian and Rician noise using different filter (**a**) ANISOTROPIC FILTER (**b**) BILATERAL FILTER (**c**) GAUSSIAN FILTER (**d**) MEAN FILTER (**e**) NON-LOCAL MEANS (**f**) MEDIAN FILTER (**g**) WAVELET FILTER (**h**) WIENER FILTER

Table 8 Comparison of Pre-processing approaches

S.No.	Filters	Original image	Denoised Gaussian image			Denoised Rician image			Denoised Gaussian and Rician image		
		PSNR	PSNR	MSE	SSIM	PSNR	MSE	SSIM	PSNR	MSE	SSIM
1.	**ANISOTROPIC FILTER**	**28.29**	**28.29**	**96.22**	**0.64**	**28.06**	**101.52**	**0.01**	**28.34**	**95.13**	**0.652**
2.	BILATERAL FILTER	28.23	28.23	97.70	0.517	27.84	106.88	0.012	28.14	99.74	0.639
3.	GAUSSIAN FILTER	28.17	28.17	98.95	0.57	27.97	103.75	0.013	28.24	97.34	0.645
4.	MEAN FILTER	28.06	28.06	101.80	0.29	28.03	102.29	0.016	28.28	96.50	0.363
5.	NON-LOCAL MEANS	28.30	28.32	95.68	0.69	28.25	97.19	0.009	28.61	89.55	0.657
6.	MEDIAN FILTER	28.05	28.05	101.80	0.48	27.91	105.03	0.011	28.07	101.27	0.475
7.	WAVELET FILTER	28.23	28.22	97.75	0.55	28.15	99.51	0.011	28.45	92.89	0.568
8.	WIENER FILTER	28.48	28.48	92.09	0.38	27.67	111.10	0.009	27.64	111.92	0.344

image. Thus, the anisotropic filter is considered to be best as its value lies in the median range i.e. neither too high nor too low.

In case of gaussian denoised image other filters have values of SSIM as 0.64 for anisotropic, 0.517 for bilateral, 0.574 for gaussian, 0.299 for mean, 0.448 for median, 0.556 for wavelet, 0.386 for wiener and the highest value is given by non-local means filter as 0.691. Further, in case of rician denoised image the values of SSIM for filters are 0.01 for anisotropic, 0.012 for bilateral, 0.013 for gaussian, 0.016 for mean and the highest value are 0.011 for median and 0.011 for wavelet, and the SSIM for wiener is 0.009 and non-local means filter is 0.009. Whereas, the SSIM for combined gaussian and rician denoised image are 0.652 for anisotropic, 0.639 for bilateral, 0.645 for gaussian, 0.363 for mean, 0.475 for median, 0.568 for wavelet and 0.344 for wiener. While, the highest value is given by the non-local means filter as 0.657. But anisotropic performs optimally with average SSIM of 0.64 for denoised gaussian noise image, SSIM of 0.01 for denoised rician noised image and SSIM of 0.652 for denoised gaussian and rician noise image. Thus, the anisotropic filter is considered to be best as its value lies in the median range i.e. neither too high nor too low.

6.6 Performance analysis of state-of-the-art segmentation approach

The experimental results for segmentation using state of the art approaches are given in Fig. 15 and Table 9.

On the basis of experimental analysis for segmentation of prostate using contour and shape-based approach, values of dice metric and area overlap is observed to be 0.49 and 0.50. Similarly, region/atlas-based approach gave 0.56 dice metric and 0.60 area overlap; whereas, thresholding gave 0.78 dice metric and 0.70 area overlap. Further, values of dice metric and area overlap for clustering-based approach were 0.82 and 0.74. Finally, deep learning-based FCN-32 gave dice metric of 0.89 and area overlap of 0.80. Thus, it can be stated that FCN-32 outperformed contour and shape based, region/atlas based, thresholding based and clustering.

6.7 Performance evaluation of classification

Performance analysis of classification was performed using different classifiers namely Support vector machine (SVM), K nearest neighbour (K-NN), Random forest (RF) and Convolutional neural network (CNN). SVM is a machine learning method which utilizes supervised learning to perform classification by plotting each data item in m-dimensional feature space. K-NN uses standard non-parametric techniques utilized for statistical pattern analysis by forming a fixed sample space. Also, RF is classification using a learning method that performs computation at training time by constructing magnitude to get the mean and mode of a class. Unlike Machine Learning (SVM, K-NN, RF), CNN operates directly on denoised images. Further, handcrafted textural features used for training machine learning classifiers were Gray level run length matrix (GLRM) and Grey level co-occurrence matrix (GLCM) extracted from the image denoised using anisotropic filter. Same set of features were used for training each classifier to avoid bias. The commonly extracted GLCM features were Autocorrelation, Joint Average, Cluster Prominence, Cluster Shade, Cluster Tendency, Contrast, Correlation, Difference Average, Difference Entropy, Difference Variance, Joint Entropy, Difference, Variance, Joint Entropy, Inverse Variance, Maximum Probability, Sum Entropy, Sum Squares and MCC. While, the GLRM features extracted here for classification includes Gray level non uniformity, Gray level non uniformity normalized, Gray level variance, High gray level emphasis, Long run emphasis, Long run high gray level

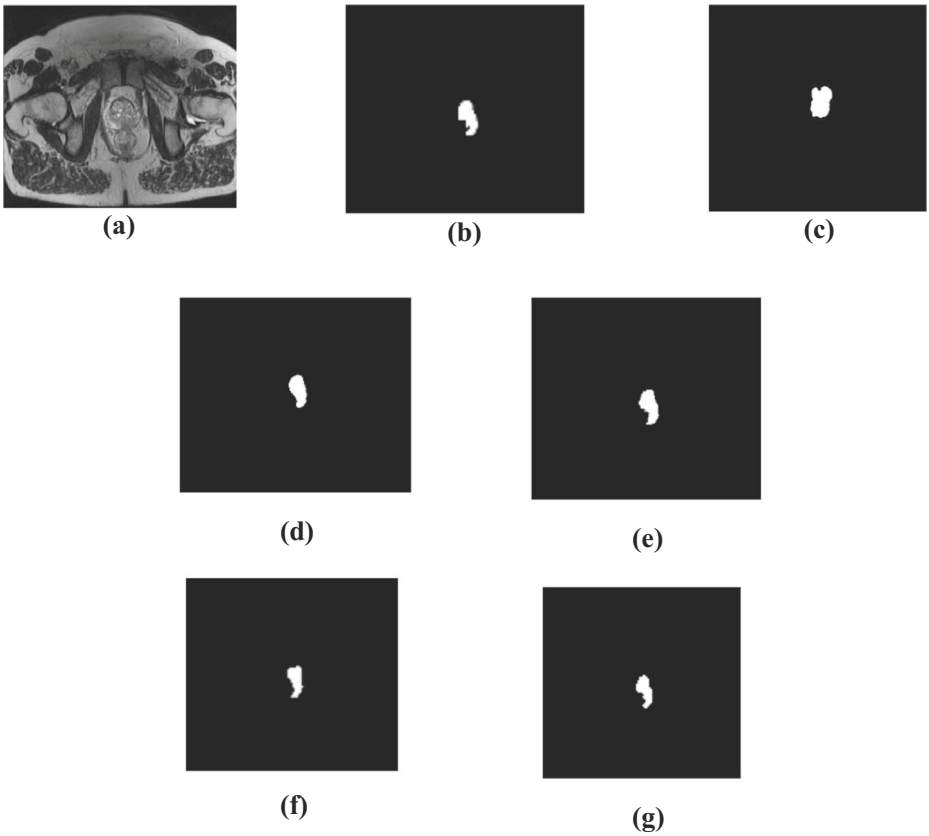

Fig. 15 Performance of Segmentation approaches (**a**) Original image (**b**) Ground truth (**c**) Contour and shape based (**d**) Region/Atlas based (**e**) Thresholding (**f**) Clustering based (**g**) FCN-32 Deep learning approach

Table 9 Performance of Segmentation approaches

Approach	Performance metric	
	Dice metric	Area overlap
Contour and shape based[a]	0.49	0.50
Region/Atlas based[b]	0.56	0.60
Thresholding based[c]	0.78	0.70
Clustering based[d]	0.82	0.74
FCN-32 Deep learning approach[e]	**0.89**	**0.80**

[a] https://github.com/mohitkumarahuja/Implementing-Active-contour-model-Snakes-Algorithm-

[b] https://github.com/anindox8/Atlas-Based-3D-Brain-Segmentation-in-T1-MRI

[c] https://github.com/himanshuRepo/2DNLMeKGSA

[d] https://github.com/ntrischi/Kmeans-Image-Segmentation

[e] https://github.com/Gurupradeep/FCN-for-Semantic-Segmentation

emphasis, Long run low gray level emphasis, Low gray level run emphasis, Run entropy, Run length non uniformity, Run length non uniformity normalized, Run percentage, Run variance, Short run emphasis, Short run high gray level emphasis, Short run low gray level emphasis.

Further, Table 10 shows the specific website links and performance analysis of different state of the art classifiers.

Based on experimental analysis, sensitivity, specificity, accuracy of SVM is found to be 87.30%, 89.34% and 85.45%. Further, K-NN shows sensitivity, specificity, accuracy of 88.91%, 88.65%, 86.57%; and RF shows 92.67% sensitivity, 90.23% specificity, 91.29% accuracy. Finally, the CNN shows sensitivity of 94.55%, specificity of 93.34%, accuracy of 94.45%. Thus, it can be concluded that deep learning-based CNN outperforms SVM, K-NN and RF.

7 Challenges and future scope

On the basis of subjective and objective analysis, various challenges are observed in the state of the art that needs to be taken into consideration to improve the accuracy of pre-processing and segmentation for classification of prostate as cancerous and non-cancerous. The preprocessing of the MRI is observed to be a major challenge as it contains certain amount of gaussian and rician noise which are removed by different filters namely curvelet, LMMSE, median, non-local means, variational level set, weighting kernel with graphics processing units, non-local PCA, thresholding, log partition along with gaussian scale and anisotropic. Also, it is compressed and dimensions are reduced to further increase the computational speed, but it leads in blurring, coarse texture and loss of image quality. Amongst the existing approaches of preprocessing, anisotropic filter proved to be optimal however in future, the hybrid approaches with use of more than one filters or deep learning-based approach could further improve the quality of image and solve the state-of-the-art problems. Besides, there is a problem of over-segmentation and under-segmentation of the prostate gland in MRI which needs to be addressed. To overcome the problems of segmentation and improve the accuracy several hybrid approaches and deep learning-based approaches can also be used in future. Moreover, the challenges in the segmentation are due to the presence of various other glands present in the nearby regions of the prostate which can be overcome by selection of the desired region of interest. Thus, there is a need of improved preprocessing, segmentation and classification approaches to diagnose the disease with improved performance. Further based

Table 10 Comparison of Classification approaches

Classifiers	Sensitivity (in %)	Specificity (in %)	Accuracy (in %)
SVM[f]	87.30%	89.34%	85.45%
K-NN[g]	88.91%	88.65%	86.57%
RF[h]	92.67%	90.23%	91.29%
CNN[i]	94.55%	93.34%	95.45%

[f] https://github.com/whimian/SVM-Image-Classification

[g] https://github.com/iampavangandhi/KNN-Image-Classification

[h] https://github.com/dhwanirc/Image-Classification-with-CNN+RF/blob/master/Image_classification%20_with%20_CNN+RF.ipynb?short_path=f814f92

[i] https://github.com/eiriniar/gleason_CNN

on recent studies performed by Karami et al. [58] in 2018, To et al. [82] in 2018, Zhu et al. [108] in 2018, Tian et al. [107] in 2018 and Hassanzadeh et al. [49] in 2019 it has been observed that all these approaches are based on deep learning for segmentation of prostate form MRI. Also, the recent approaches of classification by Ishioka et al. [56] in 2018, Yuan Y et al. [117] in 2019 and UCLA development group [111] in 2019 used deep learning networks to perform classification. Thus, current hotspot and research frontiers indicate advances of deep learning-based approaches in the current era of research for segmentation of prostate followed by its classification into malignant and benign cases in near future.

8 Conclusion

This paper presents the analysis of different denoising, segmentation and classification approaches used so far for diagnosis of prostate cancer using MRI. It summarizes challenges in the field of denoising, segmentation and classification based on the state-of-the-art approaches. Denoising filters used by researchers till date for reduction of noise suppress the significant edge details and cause blurring effect due to extra smoothness. Thus, there is a need for an improved denoising algorithm which reduces the noise without losing the significant visual information from images. While, segmentation involves other major challenges such as extraction of over or under region of interests (ROIs), computational complexity, robustness and automation. Thus, a need for a segmentation approach with less computation, automation and improved performance was encountered. Further, in the case of traditional classification, extraction of different handcrafted features varies from one study to another. Most of the studies of classification involving machine learning approach faced the problem of desirable accuracy and robustness. Although, in the current scenario use of deep learning has gained a kind attention for segmentation and classification, as it solves the problem of automation but it needs large dataset with a variety of images for training to make the classifier self-learn and perform better in testing. Studies suggested that MRI are prone to certain noise such as rician and gaussian which deteriorates the performance of further diagnosis. Although, different filters such as anisotropic, bilateral, gaussian, mean, non-local means, median, wavelet and weiner are being used in state of the art. But, on the basis of experimental analysis, it can be concluded that anisotropic filter outperforms other filters for gaussian noise with PSNR of 28.29, MSE of 96.22 and SSIM of 0.64. Also, for the rician noise anisotropic filter outperform others with PSNR of 28.06, MSE of 101.52 and SSIM of 0.01. Similarly, for the combined gaussian and rician noise, anisotropic filter outperforms others with PSNR of 28.34, MSE of 95.13 and SSIM of 0.652. Further, the segmentation includes over-segmentation and under-segmentation issues which are being addressed by different researchers till date. Thus, this study performed segmentation using a deep learning-based FCN-32, which outperformed contour and shape based, region/atlas based, thresholding based and clustering based with dice metric of 0.89 and area overlap of 0.80. Lastly, to overcome the issues of hand-crafted feature extraction and selection in traditional classifiers, classification performed using CNN offered better results than machine learning based SVM, K-NN, RF with 94.55% sensitivity, 93.34% specificity and 95.45% accuracy. Thus, the current research trend indicates use of deep learning to be a promising approach for segmentation and classification, as it doesn't require extraction of any handcrafted features. Only drawback it has is the high space complexity and time complexity for initial training, but the same can also be overcome by use of cloud computing in the near future. Further, the survey conducted state-of-the-art used comparison of machine learning approaches and only few researchers utilized deep learning approaches for comparison. However, this study could be considered cutting-edge due to

use of currently employed deep learning approaches along with traditional machine learning approaches for better analysis. Further, the manuscript gives the analysis of different modules of CAD systems such as denoising, segmentation and classification all in one place which reduces the search procedures for beginners making it easy to use.

Acknowledgments The authors are also grateful to the Ministry of Human Resource Development (MHRD), Govt. of India for funding this project(17-11/2015-PN-1) under Design Innovation Centre (DIC) sub-theme Medical Devices & Restorative Technologies.

References

1. Anonymous (2013) Automatic Diagnosis of Prostate cancer using Random Forest Classifier. https://www.cs.ubc.ca/~nando/540-2013/projects/p55.pdf
2. Abraham B, Nair MS (2018 Jan 1) Computer-aided diagnosis of clinically significant prostate cancer from MRI images using sparse autoencoder and random forest classifier. Biocybernetics and Biomedical Engineering 38(3):733–744
3. Abraham B, Nair MS (2018 Nov 1) Computer-aided classification of prostate cancer grade groups from MRI images using texture features and stacked sparse autoencoder. Comput Med Imaging Graph 69:60–68
4. Ahmed HU, Bosaily AE, Brown LC, Gabe R, Kaplan R, Parmar MK, Collaco-Moraes Y, Ward K, Hindley RG, Freeman A, Kirkham AP (2017 Feb 25) Diagnostic accuracy of multi-parametric MRI and TRUS biopsy in prostate cancer (PROMIS): a paired validating confirmatory study. Lancet 389(10071): 815–822
5. Aja-Fernandez S, Alberola-Lopez C, Westin CF (2008) Noise and signal estimation in magnitude MRI and Rician distributed images: a LMMSE approach. IEEE trans image process 17(8):1383–1398. https://doi.org/10.1109/TIP.2008.925382
6. Ali HM (2018) MRI medical image denoising by fundamental filters. In High-Resolution Neuroimaging-Basic Physical Principles and Clinical Applications 2018 Mar 14. Intech Open.
7. Alta Klinik: Multiparametric MRI of the Prostate (2019) Available at: https://www.altaklinik.com/prostate/mri-prostata/ [accessed on 28 April 2019]
8. Álvarez C, Martínez F, Romero E (2015) An automatic multi-atlas prostate segmentation in MRI using a multiscale representation and a label fusion strategy. In10th international symposium on medical information processing and analysis 2015 Jan 28 (Vol. 9287, p. 92870D). International Society for Optics and Photonics
9. Andersen AH (1995) On the Rician distribution of noisy MRI data. Magn Reson Med 34(6):910–914. https://doi.org/10.1002/mrm.1910360222
10. Anon (2019) [Online]. Available at: https://www.pcf.org/wp-content/uploads/2017/10/AN-INTRODUCTION_PROSTATE_CANCER_ GUIDE-2014.pdf [accessed on 21 Apr. 2019]
11. Anon (2019) [ebook]. Available at: https://uroweb.org/wp-content/uploads/EAU_WhitePaper_Pca_final.pdf [accessed on 21 Apr. 2019].
12. Applications and Clinical Benefits of MR Imaging | MRI Scan | Imaginis - The Women's Health & Wellness Resource Network. Imaginis.com (2019). [online] Available at: http://www.imaginis.com/mri-scan/applications-and-clinical-benefits-of-mr-imaging [Accessed on 30 April 2019]
13. Barbu A (2009) Training an active random field for real-time image denoising. IEEE Trans Image Process 18(11):2451–2462. https://doi.org/10.1109/TIP.2009.2028254
14. Bhadauria HS, Dewal ML (2013 Jul 1) Medical image denoising using adaptive fusion of curvelet transform and total variation. Computers & Electrical Engineering 39(5):1451–1460
15. Biswas R, Purkayastha D, Roy S (2018) Denoising of MRI images using Curvelet transform. InAdvances in systems, control and automation 2018 (pp. 575-583). Springer, Singapore.
16. Buades A, Coll B, Morel JM (2005) A non-local algorithm for image denoising. IEEE Comput Soc Conf Comput Vision Pattern Recogn (CVPR) 2:60–65. https://doi.org/10.1109/CVPR.2005.38
17. Burrus CS, Gopinath RA, Guo H, Odegard JE, Selesnick IW (1998) Introduction to wavelets and wavelet transforms: a primer.(Vol. 1). Prentice hall, New Jersey
18. Cammoun D, Davis KA, Hendee WR (1985 Dec) Clinical applications of magnetic resonance imaging—current status. West J Med 143(6):793–803
19. Prostate Cancer (2011) PET with ^{18}F-FDG, ^{18}F- or ^{11}C-acetate, and ^{18}F- or ^{11}C-choline. J Nucl Med 52(1):81–89

20. Candes EJ, Donoho DL (1999) Curvelets. Available from: http://www.stat.stanford.Edu/donoho/reports/1999/curvelets.pdf. Accessed on 15 September 2016
21. Chandra SS, Dowling JA, Shen KK, Raniga P, Pluim JP, Greer PB, Salvado O, Fripp J (2012 Oct) Patient specific prostate segmentation in 3-D magnetic resonance images. IEEE Trans Med Imaging 31(10):1955–1964
22. Chandra SS, Dowling JA, Shen KK, Raniga P, Pluim JP, Greer PB, Salvado O, Fripp J (2012 Oct) Patient specific prostate segmentation in 3-D magnetic resonance images. IEEE Trans Med Imaging 31(10):1955–1964
23. Chen J, Benesty J, Huang Y, Doclo S (2006 Jun 19) New insights into the noise reduction wiener filter. IEEE Trans Audio Speech Lang Process 14(4):1218–1234
24. Chilali O, Puech P, Lakroum S, Diaf M, Mordon S, Betrouni N (2016 Dec 1) Gland and zonal segmentation of prostate on T2W MR images. J Digit Imaging 29(6):730–736
25. Choyke P, Turkbey B, Pinto P, Merino M, Wood B. (2016). Data From PROSTATE-MRI. The Cancer Imaging Archive.
26. Clark T, Zhang J, Baig S, Wong A, Haider MA, Khalvati F (2017 Oct) Fully automated segmentation of prostate whole gland and transition zone in diffusion-weighted MRI using convolutional neural networks. Journal of Medical Imaging 4(4):041307
27. Ct Prostate Cancer Beach Towel for Sale by Medical Body Scans [Online]. Fine Art America (2019). Available at: https://fineartamerica.com/featured/ct-prostate-cancer-medical-body-scans.html?product=beach-towel [accessed on 27 April. 2019]
28. Das CJ, Razik A, Sharma S (2018 Jul) Positron emission tomography in prostate cancer: An update on state of the art. Indian journal of urology: IJU: journal of the Urological Society of India 34(3):172–179
29. Do MN, Vetterli M (2005) The contourlet transform: an efficient directional multiresolu-tion image representation. IEEE Trans Image Process 14(12):2091–2106. https://doi.org/10.1109/TIP.2005.859376
30. Dowling JA, Fripp J, Chandra S, Pluim JP, Lambert J, Parker J, Denham J, Greer PB, Salvado O (2011) Fast automatic multi-atlas segmentation of the prostate from 3D MR images. InInternational workshop on prostate Cancer imaging 2011 Sep 22 (pp. 10-21). Springer, Berlin, Heidelberg
31. Fehr D, Veeraraghavan H, Wibmer A, Gondo T, Matsumoto K, Vargas HA, Sala E, Hricak H, Deasy JO (2015 Nov 17) Automatic classification of prostate cancer Gleason scores from multiparametric magnetic resonance images. Proc Natl Acad Sci 112(46):E6265–E6273
32. Flores-Tapia D, Thomas G, Venugopal N, McCurdy B, Pistorius S (2008) Semi automatic MRI prostate segmentation based on wavelet multiscale products. In2008 30th annual international conference of the IEEE engineering in medicine and biology society 2008 Aug 20 (pp. 3020-3023). IEEE.
33. Francesco M, Schenone A (1999) A fuzzy clustering based segmentation system as support to diagnosis in medical imaging. Artif Intell Med 16(2):129–147
34. Gao Y, Tannenbaum A (2011) Combining atlas and active contour for automatic 3D medical image segmentation. In2011 IEEE international symposium on biomedical imaging: from Nano to macro 2011 mar 30 (pp. 1401-1404). IEEE
35. Gao Y, Tannenbaum A (2011) Combining atlas and active contour for automatic 3D medical image segmentation. In2011 IEEE international symposium on biomedical imaging: from Nano to macro 2011 mar 30 (pp. 1401-1404). IEEE.
36. Garg G, Juneja M (2016) Anatomical visions of prostate Cancer in different modalities. Indian J Sci Technol 9:44
37. Garg G, Juneja M (2018) A survey of prostate segmentation techniques in different imaging modalities. Current Medical Imaging Reviews 14(1):19–46
38. Garg G, Juneja M (2018) A survey of denoising techniques for multi-parametric prostate MRI. Multimed Tools Appl:1–34
39. Ghose S, Oliver A, Martí R, Lladó X, Vilanova JC, Freixenet J, Mitra J, Sidibé D, Meriaudeau F (2012) A survey of prostate segmentation methodologies in ultrasound, magnetic resonance and computed tomography images. Comp Methods Prog Biomed 108(1):262–287
40. Gillies RJ, Kinahan PE, Hricak H (2015 Nov 18) Radiomics: images are more than pictures, they are data. Radiology. 278(2):563–577
41. Golshan HM, Hasanzadeh RP, Yousefzadeh SC (2013 Sep 1) An MRI denoising method using image data redundancy and local SNR estimation. Magn Reson Imaging 31(7):1206–1217
42. Gonzalez RC, Woods RE (2002) Thresholding, digital image processing. Pearson Educ 59:595–611
43. Gonzalez RC, Woods RE, Eddins SL (2004) Digital image processing using MATLAB. Pearson Prentice Hall, Upper Saddle River, New Jersey
44. Gopinath N (2012 Sep) Extraction of cancer cells from MRI prostate image using MATLAB. International Journal of Engineering Science and Innovative Technology (IJESIT) 1(1):27–35
45. Guo Y, Gao Y, Shao Y, Price T, Oto A, Shen D (2014 Jul) Deformable segmentation of 3D MR prostate images via distributed discriminative dictionary and ensemble learning. Med Phys 1:41(7)

46. Guo Y, Ruan S, Walker P, Feng Y (2014) Prostate cancer segmentation from multiparametric MRI based on fuzzy Bayesian model. In2014 IEEE 11th international symposium on biomedical imaging (ISBI) 2014 Apr 29 (pp. 866-869). IEEE.
47. Guo Y, Gao Y, Shen D (2015 Dec 11) Deformable MR prostate segmentation via deep feature learning and sparse patch matching. IEEE Trans Med Imaging 35(4):1077–1089
48. Haddad RA, Akansu AN (1991) A class and image processing. IEEE Trans Fast Gaussian Binomial Filters Speech Signal Process 39(3):723–727. https://doi.org/10.1109/78.80892
49. Hassanzadeh T, Hamey LG, Ho-Shon K (2019) Convolutional neural networks for prostate magnetic resonance image segmentation. IEEE Access 7:36748–36760
50. He B, Xiao D, Hu Q, Jia F (2018) Automatic magnetic resonance image prostate segmentation based on adaptive feature learning probability boosting tree initialization and CNN-ASM refinement. IEEE Access. 6:2005–2015
51. Hossain MS, Paplinski AP, Betts JM (2018) Residual semantic segmentation of the prostate from magnetic resonance images. InInternational conference on neural information processing 2018 Dec 13 (pp. 510-521). Springer, Cham.
52. Huang T, Yang GJ, Tang G (1979) A fast two-dimensional median filtering algorithm. IEEE Trans Acoust Speech Signal Process 27(1):13–18. https://doi.org/10.1109/TASSP.1979.1163188
53. Huynh-Thu Q, Ghanbari M (2008) Scope of validity of PSNR in image/video quality assessment. Electron Lett 44(13):800–801
54. Imielinska C, Udupa J, Metaxas D, Jin Y, Angelini E, Chen T, Zhuge Y (2004) Hybrid Segmentation Methods. Principles and Practice for Segmentation, Registration, and Image Analysis, pp. 351–388
55. Isa IS, Sulaiman SN, Mustapha M, Darus S (2015 Jan 1) Evaluating denoising performances of fundamental filters for t2-weighted MRI images. Procedia Computer Science 60:760–768
56. Ishioka J, Matsuoka Y, Uehara S, Yasuda Y, Kijima T, Yoshida S, Yokoyama M, Saito K, Kihara K, Numao N, Kimura T (2018 Sep) Computer-aided diagnosis of prostate cancer on magnetic resonance imaging using a convolutional neural network algorithm. BJU Int 122(3):411–417
57. Judith Marcin M and Lam P (2018) MRI Scans: Definition uses and procedure, Medical News Today [online]. Available at: https://www.medicalnewstoday.com/articles/146309.php [Accessed on 28 April 2019].
58. Karimi D, Samei G, Kesch C, Nir G, Salcudean SE (2018 Aug 1) Prostate segmentation in MRI using a convolutional neural network architecture and training strategy based on statistical shape models. Int J Comput Assist Radiol Surg 13(8):1211–1219
59. Kaur R, Juneja M, Mandal AK (2018) Computer-aided diagnosis of renal lesions in CT images: a comprehensive survey and future prospects. Computers & Electrical Engineering. 2018 Aug 22.
60. Klosowski J, Frahm J (2017 Mar) Image denoising for real-time MRI. Magn Reson Med 77(3):1340–1352
61. LeCun Y, Bengio Y (2015 May) Hinton G. Deep learning nature 521(7553):436–444
62. Lehaire J, Flamary R, Rouvière O, Lartizien C (2014) Computer-aided diagnostic system for prostate cancer detection and characterization combining learned dictionaries and supervised classification. In2014 IEEE international conference on image processing (ICIP) 2014 Oct 27 (pp. 2251-2255). IEEE.
63. Lehmann EL, Casella G (2006). Theory of point estimation. Springer Science & Business Media.
64. Lemaitre G, Mart R, Freixenet J, Vilanova JC, Walker PM, Meriaudeau F (2015) Computer-aided detection and diagnosis for prostate cancer based on mono and multi-parametric MRI: a review. Comput Biol Med 60:8–31
65. Lemaitre G, Massich J, Martí R, Freixenet J, Vilanova JC, Walker PM, Sidibé D, Mériaudeau F (2015) A boosting approach for prostate cancer detection using multi-parametric MRI. InTwelfth international conference on quality control by artificial vision 2015 2015 Apr 30 (Vol. 9534, p. 95340A). International Society for Optics and Photonics.
66. Leventon ME, Grimson WE, Faugeras O (2002) Statistical shape influence in geodesic active contours. In5th IEEE EMBS international Summer School on biomedical imaging. 2002 Jun 15 (pp. 8-pp). IEEE
67. Li J, Weng Z, Xu H, Zhang Z, Miao H, Chen W, Liu Z, Zhang X, Wang M, Xu X, Ye Q (2018 Jan 1) Support vector machines (SVM) classification of prostate cancer Gleason score in central gland using multiparametric magnetic resonance images: a cross-validated study. Eur J Radiol 98:61–67
68. Lim JS (1990) Two-dimensional signal and image processing. Prentice hall, Englewood Cli s, NJ, pp. 710
69. Liu Y, An X (2017) A classification model for the prostate cancer based on deep learning. In2017 10th international congress on image and signal processing, BioMedical engineering and informatics (CISP-BMEI) 2017 Oct 14 (pp. 1-6). IEEE.
70. Liu X, Langer DL, Haider MA, Yang Y, Wernick MN, Yetik IS (2009 Jun) Prostate cancer segmentation with simultaneous estimation of Markov random field parameters and class. IEEE Trans Med Imaging 28(6):906–915
71. Liu P, Wang S, Turkbey B, Grant K, Pinto P, Choyke P, Wood BJ, Summers RM (2013) A prostate cancer computer-aided diagnosis system using multimodal magnetic resonance imaging and targeted biopsy

labels. InMedical imaging 2013: computer-aided diagnosis 2013 Feb 26 (Vol. 8670, p. 86701G). International Society for Optics and Photonics
72. Liu L, Yang H, Fan J, Liu RW, Duan Y (2019) Rician nowase and intensity nonuniformity correction (NNC) model for MRI data. Biomedical Signal Processing and Control. 49:506–519
73. Luisier F, Blu T, Wolfe PJ (2012) A CURE for noisy magnetic resonance images: chi-square unbiased risk estimation. IEEE Trans Image Process 21(8):3454–3466. https://doi.org/10.1109/TIP.2012.2191565
74. Macovski A (1996) Noise in MRI. Magn Reson Med 36(3):494–497. https://doi.org/10.1002/mrm.1910360327
75. Malmberg F, Strand R, Kullberg J, Nordenskjöld R, Bengtsson E (2012 Oct) Smart paint a new interactive segmentation method applied to MR prostate segmentation. MICCAI Grand Challenge: Prostate MR Image Segmentation 2012
76. Manjón JV, Coupé P, Buades A (2015 May 1) MRI noise estimation and denoising using non-local PCA. Med Image Anal 22(1):35–47
77. Martin S, Troccaz J, Daanen V (2010 Apr) Automated segmentation of the prostate in 3D MR images using a probabilistic atlas and a spatially constrained deformable model. Med Phys 37(4):1579–1590
78. Mohammadi M, Nabavi S (n.d.) Improvement in auto-contouring approaches using region growing segmentation for prostate cancer radiotherapy
79. Mohan J, Krishnaveni V, Guo Y (2013 Nov 1) MRI denoising using nonlocal neutrosophic set approach of wiener filtering. Biomedical Signal Processing and Control. 8(6):779–791
80. Nam D, Barrack RL, Potter HG (2014) What are the advantages and disadvantages of imaging modalities to diagnose wear-related corrosion problems? Clinical Orthopaedics and Related Research®. 2014 Dec 1;472(12):3665–73
81. Niaf E, Rouvière O, Mège-Lechevallier F, Bratan F, Lartizien C (2012 May 29) Computer-aided diagnosis of prostate cancer in the peripheral zone using multiparametric MRI. Phys Med Biol 57(12):3833–3851
82. Ozer S, Langer DL, Liu X, Haider MA, Van der Kwast TH, Evans AJ, Yang Y, Wernick MN, Yetik IS (2010 Apr) Supervised and unsupervised methods for prostate cancer segmentation with multispectral MRI. Med Phys 37(4):1873–1883
83. Parfait S, Walker PM, Créhange G, Tizon X, Miteran J (2012 Sep 1) Classification of prostate magnetic resonance spectra using support vector machine. Biomedical Signal Processing and Control. 7(5):499–508
84. Perona P, Malik J (1990) Scale-space and edge detection using anisotropic diffusion. IEEE Trans Pattern Anal Mach Intell 12(7):629–639. https://doi.org/10.1109/34.56205
85. Prostate Cancer Is the Leading Cancer in India: Prostate Cancer Treatment in India Cytecare (2019) [Online]. Available at: https://www.cytecare.com/blog/prostate-cancer-is-the-leading-cancer-in-india [accessed on 27 April 2019].
86. Prostate Cancer: India Against Cancer, (2019) [Online]. Available at: http://cancerindia.org.in/prostate-cancer [accessed on 27 April 2019]
87. Rajan J, Veraart J, Van Audekerke J, Verhoye M, Sijbers J (2012 Dec 1) Nonlocal maximum likelihood estimation method for denoising multiple-coil magnetic resonance images. Magn Reson Imaging 30(10):1512–1518
88. Reda I, Shalaby A, Elmogy M, Elfotouh AA, Khalifa F, El-Ghar MA, Hosseini-Asl E, Gimel'farb G, Werghi N, El-Baz A (2017 Feb 1) A comprehensive non-invasive framework for diagnosing prostate cancer. Comput Biol Med 81:148–158
89. Reda I, Khalil A, Elmogy M, Abou El-Fetouh A, Shalaby A, Abou El-Ghar M, Elmaghraby A, Ghazal M, El-Baz A (2018 May 25) Deep learning role in early diagnosis of prostate cancer. Technology in cancer research & treatment 17:1533034618775530
90. Redpath TW (1998) Signal-to-noise ratio in MRI. Br J Radiol 71(847):704–707. 10.1259/bjr.71.847.9771379
91. Rohlfing T, Brandt R, Menzel R, Russakoff DB, Maurer CR (2005) Quo vadis, atlas-based segmentation?. InHandbook of biomedical image analysis 2005 (pp. 435-486). Springer, Boston, MA.
92. Romberg JK, Choi H, Baraniuk RG (2001) Bayesian tree-structured image modeling using wavelet domain hidden Markov models. IEEE Trans Image Process 10(7):1056–1068. https://doi.org/10.1109/83.931100
93. Roth S, Black MJ (2005) Fields of experts: a framework for learning image priors. IEEE Conf Comput Vision Pattern Recogn (CVPR) 2:860–867. https://doi.org/10.1109/CVPR.2005.160
94. Rundo L, Militello C, Russo G, Garufi A, Vitabile S, Gilardi MC, Mauri G (2017 Jun) Automated prostate gland segmentation based on an unsupervised fuzzy C-means clustering technique using multispectral T1w and T2w MR imaging. Information. 8(2):49
95. Ryan O (2019) Hare, Researchers to investigate screening for prostate cancer using MRI (April 2018) [online]. Available at: https://www.imperial.ac.uk/news/185591/researchers-investigate-screening-prostate-cancer-using/ [Accessed on 28 April 2019]

96. Samiee M, Thomas G, Fazel-Rezai R (2006) Semi-automatic prostate segmentation of MR images based on flow orientation. In2006 IEEE international symposium on signal processing and information technology 2006 Aug (pp. 203-207). IEEE.
97. Sarkar S, Das S (2016) A review of imaging methods for prostate cancer detection: supplementary issue: image and video acquisition and processing for clinical applications. Biomedical engineering and computational biology. 2016 Jan;7: BECB-S34255.Table 1, A summary of clinical usage, advantages, and disadvantages across imaging modalities for pca imaging ;p.4
98. Seetha J, Raja SS (2016) Denoising of MRI images using filtering methods. In2016 international conference on wireless communications, signal processing and networking (WiSPNET) 2016 mar 23 (pp. 765-769). IEEE.
99. Shah V, Turkbey B, Mani H, Pang Y, Pohida T, Merino MJ, Pinto PA, Choyke PL, Bernardo M (2012) Decision support system for localizing prostate cancer based on multiparametric magnetic resonance imaging. Medical physics. 2012 Jul 1;39(7Part1):4093–103
100. Sharma KK, Gurjar D, Jyotyana M, Kumari V (2019) Denoising of brain MRI images using a hybrid filter method of Sylvester-Lyapunov equation and non local means. InSmart innovations in communication and computational sciences 2019 (pp. 495-505). Springer, Singapore.
101. Smith CP, Czarniecki M, Mehralivand S, Stoyanova R, Choyke PL, Harmon S, Turkbey B (2018 Jun) Radiomics and radiogenomics of prostate cancer. Abdominal Radiology 20:1–9
102. Smith-Bindman R (2010 Jul 1) Is computed tomography safe. N Engl J Med 363(1):1–4
103. Subudhi BN, Thangaraj V, Sankaralingam E, Ghosh A (2016 Nov 1) Tumor or abnormality identification from magnetic resonance images using statistical region fusion based segmentation. Magn Reson Imaging 34(9):1292–1304
104. Sudeep PV, Palanisamy P, Kesavadas C, Rajan J (2015 Jul 1) Nonlocal linear minimum mean square error methods for denoising MRI. Biomedical Signal Processing and Control. 20:125–134
105. Tian Z, Liu L, Fei B (2015) A supervoxel-based segmentation method for prostate MR images. InMedical imaging 2015: image processing 2015 mar 20 (Vol. 9413, p. 941318). International Society for Optics and Photonics
106. Tian Z, Liu L, Zhang Z, Fei B (2016 Mar) Superpixel-based segmentation for 3D prostate MR images. IEEE Trans Med Imaging 35(3):791–801
107. Tian Z, Liu L, Zhang Z, Fei B (2018 Jan) PSNet: prostate segmentation on MRI based on a convolutional neural network. Journal of Medical Imaging. 5(2):021208
108. To MN, Vu DQ, Turkbey B, Choyke PL, Kwak JT (2018 Nov 1) Deep dense multi-path neural network for prostate segmentation in magnetic resonance imaging. Int J Comput Assist Radiol Surg 13(11):1687–1696
109. Trigui R, Mitéran J, Walker PM, Sellami L, Hamida AB (2017 Jan 1) Automatic classification and localization of prostate cancer using multi-parametric MRI/MRS. Biomedical Signal Processing and Control 31:189–198
110. Tustison NJ, Gee JC (2009) Introducing dice, Jaccard, and other label overlap measures to ITK. Insight J 2009 Jul;2.
111. Ucla technology development group (2019) University of californiaedu. [Online]. Available from: https://techtransfer.universityofcalifornia.edu/NCD/29986.html [Accessed 30 April 2019]
112. Wang Z, Bovik AC, Sheikh HR, Simoncelli EP (2004) Image quality assessment: from error visibility to structural similarity. IEEE Trans Image Process 13(4):600–612
113. Wang X, Yang W, Weinreb J, Han J, Li Q, Kong X, Yan Y, Ke Z, Luo B, Liu T, Wang L (2017 Nov 13) Searching for prostate cancer by fully automated magnetic resonance imaging classification: deep learning versus non-deep learning. Sci Rep 7(1):15415
114. Weiss Y, Freeman WT (2007) What makes a good model of natural images?. In: IEEE conference on computer vision and pattern recognition (CVPR) (pp 1-8). Doi: https://doi.org/10.1109/CVPR.2007.383092
115. Yang X, Liu C, Wang Z, Yang J, Le Min H, Wang L, Cheng KT (2017 Dec 1) Co-trained convolutional neural networks for automated detection of prostate cancer in multi-parametric MRI. Med Image Anal 42: 212–227
116. Yuan J (2018 Nov 1) An improved variational model for denoising magnetic resonance images. Computers & Mathematics with Applications 76(9):2212–2222
117. Yuan Y, Qin W, Buyyounouski M, Ibragimov B, Hancock S, Han B, Xing L (2019 Feb) Prostate cancer classification with multiparametric MRI transfer learning model. Med Phys 46(2):756–765
118. Zhu Y, Williams S, Zwiggelaar R (2007 Jun 1) A hybrid ASM approach for sparse volumetric data segmentation. Pattern recognition and image analysis 17(2):252–258
119. Zhu H, Li Y, Ibrahim JG, Shi X, An H, Chen Y, Gao W, Lin W, Rowe DB, Peterson BS (2009) Regression models for identifying noise sources in magnetic resonance images. J Am Stat Assoc 104(486): 623–637. https://doi.org/10.1198/jasa.2009.00299

120. Zhu W, Zeng N, Wang N (2010) Sensitivity, specifcity, accuracy, associated confdence interval and ROC analysis with practical SAS implementations. NESUG Proc 14(19):67
121. Zhu Y, Wei R, Gao G, Ding L, Zhang X, Wang X, Zhang J (2019 Apr) Fully automatic segmentation on prostate MR images based on cascaded fully convolution network. J Magn Reson Imaging 49(4):1149–1156

Affiliations

Mamta Juneja[1] · Sumindar Kaur Saini[1] · Jatin Gupta[1] · Poojita Garg[1] · Niharika Thakur[1] · Aviral Sharma[1] · Manan Mehta[1] · Prashant Jindal[1]

✉ Prashant Jindal
jindalp@pu.ac.in

Mamta Juneja
mamtajuneja@pu.ac.in

Sumindar Kaur Saini
sumindarkaursaini@gmail.com

Jatin Gupta
jatingupta1595@gmail.com

Poojita Garg
poojita8garg@gmail.com

Niharika Thakur
niharikathakur04@gmail.com

Aviral Sharma
100aviral100@gmail.com

Manan Mehta
manan161200@gmail.com

[1] University Institute of Engineering and Technology, Panjab University, Chandigarh, India